RIGA TECHNICAL UNIVERSITY

Luca Piacentini

MECHANICAL DESIGN AND OPTIMIZATION OF A SUPPORTING SYSTEM FOR CRYOGENIC DEVICES UNDER VARIABLE LOADS: THE STUDY CASE OF A CARBON ION ROTATING GANTRY FOR MEDICAL TREATMENTS

Summary of the Doctoral Thesis

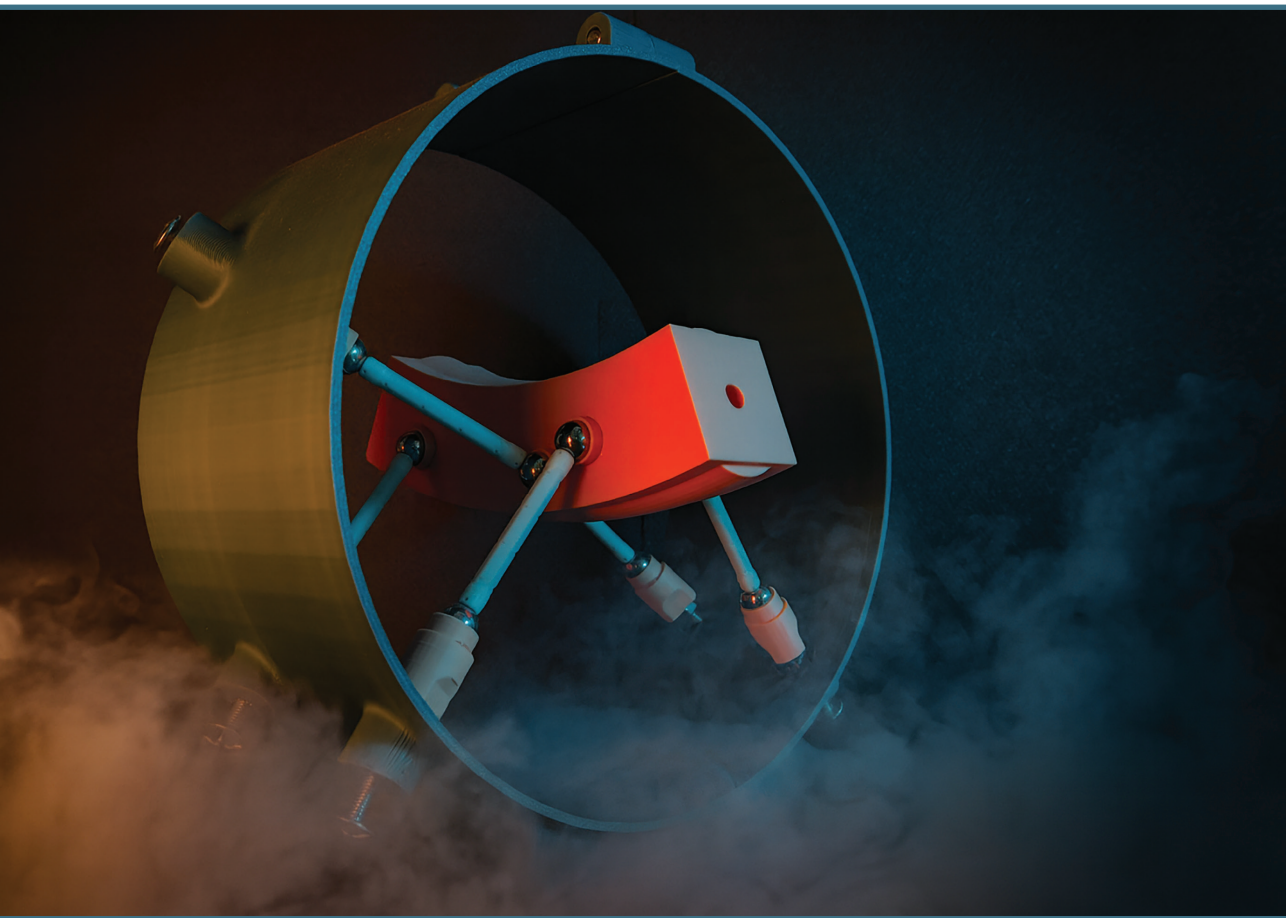

RTU Press
Riga 2025

RIGA TECHNICAL UNIVERSITY

Faculty of Natural Sciences and Technology
Institute of Particle Physics and Accelerator Technologies

Luca Piacentini
Doctoral Student of the Study Programme:
"Particle Physics and Accelerator Technologies"

MECHANICAL DESIGN AND OPTIMIZATION OF A SUPPORTING SYSTEM FOR CRYOGENIC DEVICES UNDER VARIABLE LOADS:

THE STUDY CASE OF A CARBON ION ROTATING GANTRY FOR MEDICAL TREATMENTS

Summary of the Doctoral Thesis

Scientific Supervisors

Professor Dr. sc. eng. TOMS TORIMS
Dr. sc. eng. LUCA DASSA
Professor Dr. sc. eng. STEFANO UBERTI

RTU Press
Riga 2025

Piacentini, L. Mechanical Design and Optimization of a Supporting System for Cryogenic Devices under Variable Loads: The Study Case of a Carbon Ion Rotating Gantry for Medical Treatments. Summary of the Doctoral Thesis. – Riga: RTU Press, 2025, 49 p.

Published in accordance with the decision of the Promotion Council "RTU-04" of 4 july, 2025, Minutes No. 04030-9.4/1.

AKNOWLEDGEMENTS

I would like to express my deepest gratitude to my supervisors, Dr. Luca Dassa, Prof. Toms Torims, and Prof. Stefano Uberti, who guided me throughout my doctoral research, conducted at both CERN and Riga Technical University. I am sincerely thankful for everything they have taught me, and for their invaluable advice on how to grow not only as a researcher but also as a professional and as a person. I am also grateful to Dr. Maurizio Vretenar, the leader of the NIMMS initiative at CERN, and to Prof. Toms Torims, Prof. Kārlis Dreimanis, and Dr. Andris Ratkus, members of IPPAT, for the financial support that enabled me to carry out my research at CERN. My thanks extend as well to the EN-MME group at CERN and to UNIBS, for making it possible for Dr. Luca Dassa and Prof. Stefano Uberti to supervise my work. Finally, I wish to thank my family and friends for their unhesitating and tireless support throughout this four-year journey across Europe despite the thousands of kilometers that often separated us.

Cover Picture by *Luca Piacentini*.
https://doi.org/10.7250/9789934372292
ISBN 978-9934-37-229-2 (pdf)

DOCTORAL THESIS PROPOSED TO RIGA TECHNICAL UNIVERSITY FOR PROMOTION TO THE SCIENTIFIC DEGREE OF DOCTOR OF SCIENCE

To be granted the scientific degree of Doctor of Science, the present Doctoral Thesis has been submitted for defence at the open meeting of RTU Promotion Council on December 12, 2025, at 11.00, Zoom online https://rtucloud1.zoom.us/j/94276909347.

OFFICIAL REVIEWERS

Dr. sc. Eng. Olga Kononova,
Riga Technical University

Dr. sc. Alberto Degiovanni
Riga Technical University

Dr. sc. Florent Cosandier
École Polytechnique Fédérale de Lausanne, Switzerland

Dr. sc. Eduardo Cano Pleite
University of Madrid, Spain

DECLARATION OF ACADEMIC INTEGRITY

I hereby declare that the Doctoral Thesis submitted for review to Riga Technical University for promotion to the scientific degree of Doctor of Science is my own. I confirm that this Doctoral Thesis has not been submitted to any other university for promotion to a scientific degree.

Luca Piacentini ..... (signature)
Date: .....

The Doctoral Thesis has been written in English. It consists of an Introduction; 8 Chapters; Conclusion; 74 figures; 39 tables; 4 appendices; the total number of pages is 169, including appendices. The Bibliography contains 114 titles.

Contents

1. Outline of the Thesis

1.1. General context of the Thesis

Cryogenic devices are specialized systems operating at extremely low temperatures, from 1.8 K to 125 K. They are used in scientific research, industrial production, and advanced technological applications. In high-energy physics experiments, most particle accelerator components are cryogenic devices. Other applications include superconducting generators for wind turbines, satellites, aerospace systems, and societal uses such as superconducting magnets for certain cancer treatments.

Typically, all cryogenic devices require the implementation of an essential set of subsystems:

- Cooling system maintains the cryogenic temperature. For superconducting elements, its primary function is to keep coil materials in a superconducting state (typically 1.9–5 K).
- External vacuum vessel insulates the device from the environment, eliminating convective heat transfer and limiting contamination. It also ensures low humidity and minimal polluting agents inside the device.
- Internal supports hold the device in its correct position and resist loads during operation.
- Thermal screen envelopes the cryogenic device at a distance, blocking direct radiative heat transfer from the vacuum vessel at room temperature to the cold device. It is actively cooled to an intermediate temperature and often integrates thermalizations that split internal supports, acting as heat sinks to intercept conduction heat flow.

The design of the supporting system for a cryogenic device requires to satisfy four main requirements:

- ensure functionality for the cryogenic device by holding it in the correct position;
- grant sufficient rigidity in order to reduce elastic deformations and accuracy losses due to loads;
- minimize the heat-flux through the supports, which results in a reduction of running costs for the cryogenic cooling system;
- align the cryogenic device at warm during the passive alignment phase and in special cases also at nominal cryogenic temperatures to ensure higher levels of position accuracy.

In research and high-tech applications, the performance of cryogenic devices often depends on their positional accuracy under load. Literature shows that most support designs address static loads, with positional errors corrected during a passive alignment phase at room temperature before cool-down. Dynamic loads such as earthquakes or vibrations are rarely considered, and when they are, they typically have little influence on the support design. However, under variable loads that cause continuous displacement of the cold mass, passive alignment cannot compensate for position errors, making the study of support stiffness and arrangement of crucial importance.

The literature analysis highlighted the lack of clear documented scientific knowledge about the combined area of study of cryogenic device supporting systems, precise positioning and variable loads. Additionally, in literature rarely are presented formalized mathematical models to study the internal actions on the supports of a cryogenic device under loads. Such models lack also generality and rely on the assumption of a symmetric support configuration. Furthermore, no model has been found for a mathematical model able to predict displacements of the cryogenic device under loads.

The study case of a superconducting C-ion gantry for medical treatments falls entirely in the previously mentioned knowledge gap and will be used in this Thesis as an example to develop models that can be applied also on different applications. This Thesis proposes to study only rod-supporting systems, because these have been found to be the most commonly used in documented static cases. Additionally, the use of rod supporting systems enables to have mainly axial loads on the supports, reducing the need of greater cross-sections that would be necessary to reduce the stress due to other internal actions, i.e. shear.

1.2. Goals and tasks of the Thesis

This Thesis aims to develop a novel method for the optimal mechanical design of supporting systems for a cryogenic device under variable loads.

The specific case of superconducting magnets on a rotating gantry for medical applications serves as a case study to use for the first time the developed tools, with the goal of achieving an optimal design for the supporting system.

To reach this goal this Thesis is structured around the following tasks:

1. Reviewing the literature on existing supporting systems for cryogenic devices, identifying their characteristics, common design approaches, and research gaps worth exploring.
2. Proposing different supporting architectures to ensure a comprehensive study of the problem.
3. Defining the requirements and load cases for the supporting system under variable loads.
4. Developing general mathematical models to analyze supporting systems under variable loads.
5. Establishing relevant criteria for comparing different support system designs.
6. Designing and optimizing each supporting system by selecting its architecture, material, and geometry.
7. Evaluating the proposed solutions against the defined criteria.

1.3. Scope of the Thesis

The mathematical models developed in this Thesis are applicable to supporting systems consisting of six or more thin supports, of any geometry and material but joined at each end by spherical or universal joints, inhibiting the development of internal actions other than the axial component. The models are applicable at supports that can exhibit a thermal gradient through the supports. The models have been validated by comparing the predictions with those of standard finite element simulation software and not through testing campaigns, as the cost of a full scale system is estimated around two millions of Swiss francs, and a simplified scaled down version around 100,000 Swiss francs.

1.4. Statements of the Thesis

The following are the statements that this Thesis aims to prove:

1. Mathematical models of pose (position and orientation) and internal actions of statically determinate (6 supports) and indeterminate rod supporting systems (any number of supports > 6) for cryogenic devices under variable external loads can be formulated and provide simple understanding of the complex system.
2. Mathematical models provide results as accurate as finite element analysis (*FEA*).
3. Models are computationally cheaper than *FEA*.
4. Developed tools can be used to find an optimal design for the supporting system of superconducting magnets on a C-ion gantry beam line for medical applications.

1.5. Scientific novelty and practical applications

The scientific novelty of this Thesis lies in the proposal of a structured and complete approach to study rod supporting systems of cryogenic devices subject to variable loads both in direction and intensity providing mathematical models that are of general use and can be applied to multiple applications.

The hypothesis is that by formulating mathematical models to study both statically determinate and indeterminate supporting systems the problems can be studied in a comprehensive way. Additionally, the proposal of such models can reduce the computational cost of commonly used finite element analysis widely used in the field of cryogenic devices. Such reduction in computational cost can lead to machine-based optimizations routine, improving performances of supporting systems, and large scale sensitivity studies, addressing the impact of key parameters variations to the system performances.

Proving the mentioned hypothesis can have a significant impact on hadron therapy technology, medical imaging systems, and various other fields, including superconducting generators for wind turbines, superconducting radio frequency cavities, optical alignment systems for cryogenic devices such as high-energy physics experimental apparatus, and satellites, ultimately contributing to societal advancements.

1.6. Scientific methodology and tools

The literature review analyzed cryogenic device support systems using advanced searches in Google Scholar. A structured approach is proposed for studying support systems under highly variable loads, with a focus on superconducting magnets in a rotating gantry while ensuring general applicability. Both statically determinate and indeterminate solutions are explored within the framework of structural mechanics.

To mitigate human bias when comparing solutions of differing complexity (one with 16 free parameters and the other with 6), a machine-driven optimization coded in *Wolfram Mathematica* is employed. This approach, based on mathematical models, reduces computational costs compared to finite element analyses (*FEAs*). Lumped parameter models (*LPMs*) are selected for their ability to capture system behavior with a minimal set of key parameters, significantly improving optimization efficiency.

The *LPM* for the statically determinate solution is adapted from an existing model in parallel mechanisms, while the *LPM* for the statically indeterminate solution is derived from the principle of virtual work. Their accuracy is benchmarked against *Ansys® Workbench 2022 R2* using 3D models created in *SolidWorks*.

Comparison criteria focus on machine functionality, including accuracy losses during operation, heat flux through supports, sensitivity to manufacturing tolerances and preload variations, safety factors for transportation and handling, and vibration frequencies.

Data analysis and visualization are conducted using *Wolfram Mathematica* and *Microsoft Excel*.

1.7. List of publications

Publications directly related to the Thesis topic:

1. **Piacentini, L.**, Dassa, L., Perini, D., Ratkus, A., Torims, T., & Uberti, S. (**2025**). Lumped Parameter Model for Structural Analysis of Over-Constrained Multi-Legged Parallel Mechanism Supporting System Applied to Cryogenic Devices. **Machines**, 13(2). ..... DOI:10.3390/machines13020129.
2. **Piacentini, L.**, Dassa, L., Perini, D., Ratkus, A., Torims, T., & Uberti, S. (**2024**). Design of a 6-supports exactly constrained supporting system for superconducting magnets and its application to rotating gantries for cancer therapy. **Meccanica** 59, 2203–2226. ..... DOI:10.1007/s11012-024-01896-x
3. **Piacentini, L.**, Dassa, L., Perini, D., Ratkus, A., Torims, T., & Uberti, S. (**2023**). Literature Review of Suspension Systems for Superconducting Elements. **Machines**, 11, 929. ..... DOI:10.3390/machines11100929
4. Pullia, M.G., Felcini, E., Benedetto, E. et al. (**2024**). Gantries for carbon ions. **Health Technology**. 14, 973–983. ..... DOI:10.1007/s12553-024-00870-7

List of all publications available at ResearchGate.

1.8. Approbation of the research results

List of conferences:

1. **IPAC. 2025.** Taipei. Poster presentation: Layout optimization and comparison of a Carbon-ion gantry based on different mechanical structures. (Abstract accepted).
2. **ICEC. 2024.** Geneva. Poster title: Cold Mass Suspension System of a Rotating Gantry for Medical Applications. ..... Link.
3. **CBC. 2024.** Tallinn. Oral presentation: Design of a Supporting System for Superconducting Magnets and its application to Rotating Gantries for Cancer Therapy. ..... Link.
4. **CBC. 2023.** Riga. Poster presentation: Mechanical design of the suspension system of superconducting elements subject to variable loads. ..... Link.
5. **CBC. 2022.** Vilnius. Oral presentation: Advancements of integration and mechanical design of gantries for ion-therapy. ..... Link.

List of seminars and project meetings:

1. **CERN NIMMS. 2024.** Geneva. Project meeting. C-ions gantry mechanical design and integration. ..... https://indico.cern.ch/event/1487497/.
2. **CERN EN-MEE. 2024.** Geneva. Student seminar. Desing of a suspension system for a cold mass on a rotating gantry for medical applications.
3. **CERN MAPF. 2024.** Geneva. Project meeting. Mechanical integration of C-ion gantry. https://indico.cern.ch/event/1346853/
4. **CERN EN-MEE. 2023.** Geneva. Student seminar. Study on the suspension system of superconducting magnets for hadron therapy rotating gantries.
5. **CERN MAPF. 2023.** Geneva. Project meeting. Mechanical integration of C-ion gantry. https://indico.cern.ch/event/1217564/

2. Literature analysis of supporting systems for cryogenic devices

Superconducting materials require extremely low temperatures, typically between 1.8–4.5 K, making heat extraction increasingly costly as temperatures decrease. Any connection between the superconducting cold mass and the room-temperature environment introduces heat inflow, yet some connections, such as the supporting system, are essential for functionality. These supports must ensure mechanical resistance to various operational loads while minimizing heat transfer. Consequently, their design involves trade-offs between structural integrity and thermal efficiency. Engineers have developed recurring design patterns in geometry and materials to address this challenge. This chapter provides an overview and classification of these solutions.

2.1. Literature analysis methodology

The Open Access database used for searching scientific articles is connected to the Google Scholar browser [1]. The time frame has been limited to the most recent results available as of February 2023. Search operators were used to refine the research as follows:

- the "*word*" operator is used to include a specific word or sentence in the search;
- parentheses, *AND*, and *OR* operators follow the common Boolean algebra;
- the $\sim$ operator allows the browser to search for synonyms of a word;
- the "-" operator excludes a word from the results;
- the "*intitle*": operator forces the browser to find results that contain a specific word in the title.

"*FEA*" was used to filter results in which the supporting system has been analyzed thoroughly, recognizing the importance of *FEA* in a mechanical study. "superconducting" sets the search field to superconducting technologies. "cold mass" highlights the interest in general cold mass supports. "mechanical" filters for mechanical analysis rather than just general physics analysis. "support" sets the search field to the supports of a superconducting element. "suspension" used to search for synonyms of support. "*ATLAS*", "*CMS*", and "*LHC*" are used as exclusions to filter out recurring articles referencing two of the most well-known physics experiments and the most famous accelerator in the world. Publications specifically related to *LHC* supports have been included manually. The search returned 194 results, which were examined for images of supporting systems, their descriptions, and *FEA* results. When an article's content was incomplete, related publications were explored for additional information.

This literature review aimed to highlight the following characteristics of the supporting system:

- the architecture, i.e, the arrangement of supports with respect to the superconducting body;
- the geometry of the single supporting element of the supporting system;
- the materials used for the supporting element;
- the characteristics of the supported body, such as its mass and length;
- the cool-down effect, i.e, the kinematic behavior of the architecture when the superconducting body undergoes a thermal cycle;

- the adjustability and classification of the adjustment system.

The most relevant results have been reported and comprehensively analyzed in the full Thesis text. This summary reports a compact version of the summary table (Table 2.1) classifying the supporting systems.

Table 2.1

Summary table of the researched suspension system for superconducting elements.

Ref.	Project	Element	SC material	Mass kg	Architecture	Material	Status [a]
[2], [3]	*SSRF*	Magnet	NbTi wire	160	8 bands	*CFRP*	op.
[4]–[7]	*ESS*	Cavity	Nb sheets	210	8 rods + 1 post ***	Ti-6Al-4V (rod) + power-coupler	const.
[8]–[10]	*HL-LHC*	Cavity	Nb bulk	250	2 blades + 1 post	SS 316L + power-coupler	dev.
[11]–[13]	*SPL*	Cavity	Nb bulk		2 *ICS* + 1 post		ND
[6] [14]–[16]	*ESS* (spoke)	Cavity	Nb sheets		22 rods + 2 posts	Ti-6Al-4V (rod) + power-coupler	const.
[17]	*VECC*	Magnet	Bi-2223 wire		4 bands	G10	op.
[18]	*CAS*	Magnet	YBCO tape		8 pillars	G10	dev.
[19]	*MDS* (*UT*)	Magnet	NbTi wire	520	4 posts + 4 rods	G11	dev.
[20], [21]	*HIE-ISOLDE*	Frame	Cu sheets Nb coating	850	2 rods + 2 plates		op.
[22]	*IHEP*	Magnet		1400	8 bands	T300 (*CFRP*)	op.
[23], [24]	*TLS*	Magnet	NbTi wire		8 bands	*UFGE*	op.
[25]	*MICE*	Magnet	NbTi wire	1600	8 bands	*UFGE*	op.
[26], [27]	*FAIR*	Frame	NbTi wire		8 rods	Ti-6Al-4V + AISI 304	const.
[28], [29]	*Mu2e*	Magnet	NbTi wire		3 springs + 14 rods	Inconel® 718	const.
[30], [31]	*RHIC*	Magnet	NbTi wire	3605	3 posts	Ultem® 2100 or SEl-GFN3 Noryl®	op.
[32]	*CAS*	Magnet		4000	8 bands		res.
[33]	*ATLAS CS*	Magnet	NbTi wire	4700	24 struts	*GFRE*	op.
[34], [35]	*SSC*	Magnet	NbTi wire	7700	5 posts	*G11CR*	cancelled
[36], [37]	*LCLS-II*	HE pipe	Nb sheets	8600	3 posts (hung)	G10	op.
[38], [39]	*ITER*	Feeder		10,000 ca.	2 posts	SS 316LN	const.
[40]–[43]	*LHC*	Magnet	NbTi wire	25,000 **	3 posts **	*GFRE*	op.
[44]–[46]	*ATLAS BT*	Magnet	NbTi wire	45,000	8 rods + 32 stops	Ti 5Al 2.5 Sn *ELI* *GFRE*	op.
[47]–[49]	NeuroSpin	Magnet	NbTi wire	132,000	8 rods	Ti-6Al-4V	comm.
[50]–[52]	*ATLAS ECT*	Magnet	NbTi wire	160,000	20 rods	stainless steel	op.
[53]	*CMS CS*	Magnet	NbTi wire	225,000	30 rods	Ti 5Al 2.5Sn *ELI*	op.

Table 2.1

Continuation

Ref.	Project	Element	SC material	Mass kg	Architecture	Material	Status [a]
[54], [55]	*ITER*	Magnet	Nb3Sn and NbTi	23×10^6	18 multi-blades	stainless steel	const.
[56]	*DEMO*	Magnet	Nb3Sn, NbTi and RE-123		16 multi-blades	stainless steel	dev.

The main characteristics have been reported and classified following the nomenclature reported as notes below the table. Results have been ordered by increasing weight of the cold mass. a. – status at the beginning of 2023. dev. – in development; const. – in construction; comm. – in commissioning; op. – operational; res. – for research only. ** Data of cryodipoles, not of *SSS*. *** The post is represented by the power coupler, able to slide vertically but fixed radially in this case.

2.2. Discussion

Research on supporting systems for cold masses has led to over 20 applications, including accelerating cavities, wiggler magnets, magnetic density separators, solenoids, quadrupoles, dipoles, feeders, detector magnets, and *MRI*. The suspended mass ranges from 160 to 23×10^6 kg, with axial lengths between 0.3 m and 25 m (see Table 2.1).

Three main suspension architectures have been identified:

- multi-post – used for slender, heavy bodies like synchrotron cryomagnets (*LHC*, *RHIC*, *SSC*), minimizing vertical sagitta with few penetrations of the vacuum vessel;
- 8-support – mostly used for lighter or bulkier bodies;
- cavity architecture – supports cavities using the *FPC* tube wall as a post with additional stiffening.

Other specialized solutions exist for high-curvature solenoids (*Mu2e*), pancake-shaped separators, and detector magnets.

Common cool-down behaviors have been classified: some systems introduce additional stress to ensure precise positioning post-cooling, while others accept asymmetric contraction to reduce stress. An optimized approach, as seen in *FAIR*, tunes materials and geometry to achieve symmetric contraction without extra stress.

Supporting materials fall into metallic (titanium, stainless steel, nickel-chromium alloys) and composite (glass and carbon fiber-reinforced polymers) categories, balancing mechanical resistance and thermal efficiency. A correlation exists between material and support shape: metallic rods dominate, while double-band architectures favor composites, except for G11 rods in a *UT* magnetic density separator.

Two recurring adjustability solutions exist based on error-chain tuning:

- *SVI*: Adjustment between cold mass supports and the vacuum vessel.
- *VGI*: Adjustment between the vacuum vessel and rigid ground.

Literature designs focus on nominal conditions, primarily counteracting dead weight and electromagnetic forces. Non-nominal scenarios like transport loads, seismic events, and quenching failures are considered, but mainly in terms of mechanical resistance, without constraining system rigidity. Cold mass misalignment is corrected during assembly, leaving stiffness unconstrained.

For variable loads, such as in gantries, full passive compensation of misalignment is impossible across all positions. Adjustments at one angle may negatively affect others,

shifting the design trade-off from heat load versus mechanical resistance to include stiffness constraints. This necessitates research into architectures suitable for rotating machines. While existing solutions could be adapted, further analysis is required.

SVI systems, featuring bilateral fixtures like rod ends and spherical bearings, are better suited for rotating applications. *VGI* systems, which use unilateral fixtures (e.g., spherical washers), require further *R&D*. Adding *SVI* regulation for post-supported bodies complicates the cryostat assembly and decreases performances (stiffness) of the tuning system itself.

Structures can be classified as statically determinate or indeterminate depending on the number and type of joints and bodies involved. Statically determinate systems are easier to automate because joint movements do not cause internal stress. In contrast, statically indeterminate (over-constrained) systems are more complex to automate. All systems found in the literature, except the one used in *ISOLDE*, are statically indeterminate. Even in *ISOLDE*, the motorized struts only allow adjustment in four degrees of freedom, meaning full automation is not achieved. Thus, there is a clear knowledge gap in the literature regarding fully constrained and automated supporting systems, which this Thesis aims to address.

The literature review revealed a lack of existing solutions for supporting systems of cryogenic devices under highly variable loads, especially in medical applications like gantries. While recurring designs exist for static-load cases (e.g., superconducting magnets, *RF* cavities), no examples were found for dynamic applications. Moreover, studies rely heavily on *FEA* and lack formal mathematical modeling.

A conceptual transferability analysis shows that current systems are not designed for variable-load contexts, pointing to new research opportunities. Among them, the eight-support architecture appears promising for redesign as a statically indeterminate system suited to variable loads, such as in medical gantries. Simultaneously, there is no documented research on statically determinate support and alignment systems with full 6 *DOF* control, marking a complete gap in knowledge.

Addressing these gaps could have significant value in hadron therapy machines, as well as in superconducting generators for wind turbines, *RF* cavities, cryogenic alignment systems in high-energy physics, and satellites.

3. Research framework for the development of supporting systems of cryogenic devices

The literature analysis highlights the absence of a dedicated solution for cryogenic device supports under highly variable loads. Additionally, the field lacks completeness, as no statically determinate solutions were found, and it relies solely on *FEA*s without a general mathematical formalism.

This chapter introduces the structured approach used in this Thesis. It initially examines the approach taken to resolve the completeness gap. The optimization approach is then discussed to mitigate human bias in solution selection. Design requirements and load cases for the gantry are outlined, followed by the formulation of mathematical models to establish a formal framework. Relevant comparison metrics are introduced to evaluate solutions, and finally, the tools used in this study are listed.

3.1. Design objectives of the Thesis

In structural mechanics, structures are classified as *statically determinate* or *statically indeterminate*. Generally, statically indeterminate structures are stiffer and stronger as well as intrinsically redundant. However, changes, such as displacements generated by thermal contraction, typically generate additional stresses in the structure.

The literature analysis conducted [57] and reported in Chapter 2 of the Thesis highlighted the lack of completeness in designing the supporting system for a cryogenic device, analyzing mostly statically indeterminate (or over-constrained) supporting architectures. The few cases found in literature have been judged non transferable to an application where loads are highly variable. With the aim of studying in a comprehensive way the supporting system of a cryogenic device subject to variable loads, this study will consider both statically determinate and indeterminate solutions, discussing the possible architectures in Chapter 4 of the Thesis.

3.2. Optimization approach of supporting systems

The optimization approach choice depends on the structural nature and desired characteristics of the architecture. Statically indeterminate systems often use symmetric support arrangements, simplifying the number of free parameters, thus, the optimization process. In contrast, exactly constrained systems can have more parameters, making optimization more complex. To avoid human bias in comparing systems with different level of complexity, this study will use a machine-driven optimization approach.

Optimization in mechanics typically relies on two methods: *FEA* (finite element analysis), used for complex structures, and analytical models, used for simpler geometries. *FEA* involves meshing complex geometries and solving equilibrium equations, with accuracy depending on mesh size. Analytical models are faster due to fewer bodies involved, making them advantageous for optimization. This Thesis will explore machine-driven optimization using analytical models.

3.3. Design requirements for supporting systems

Having chosen a machine-driven optimization base on analytical models, it is important to analyze the minimum parameters to be introduced in such models. Hence, the

main requirements for the design are listed and described in Table 3.1, taking the study case of the gantry as an example.

Table 3.1

The basic requirements for the design of the supporting system of the superconducting elements on a gantry

Category	Requirement	Description	Priority
Functionality	Accuracy	The pose (position and rotation) of the cold mass, measured at its geometrical center, must be within $\pm 0.6\,\text{mm}$ (3σ) or $\pm 0.6\,\text{mrad}$ (3σ) for all six *DOF* (degrees of freedom) at each gantry angular position	higher
	Alignment	The supporting system must correct positioning errors of the geometrical center of the cold mass up to $\pm 20\,\text{mm}$ and $\pm 20\,\text{mrad}$ along any direction	high
	Thermal insulation	The supporting elements must insulate the cold mass from external environment conductive heat loads, minimizing them	high
Structural integrity	Mechanical resistance	The system must withstand loads encountered during the phases of the product	high
	Vibration	Natural vibration frequencies of the supporting architecture must not be excited by expected external excitation	normal
	Environment compatibility	The system components must operate at cryogenic temperatures (4.5 K) and in a radiation environment	high
Geometry	Compactness	The supporting system must not exceed 1.8 m in width	good to have
	Lightness	The cryostat must be under 1.5 t	good to have
Production	Feasibility	Standard manufacturing technologies should be applied, and commercial parts used as much as possible	good to have

The design requirements have been assigned a priority level for the satisfaction of requirements. The priority levels associated with each requirement have been listed in Table 3.1.

3.4. Load cases

Functionality and structural integrity must be ensured for the following types of loads: nominal loads during the operation of the gantry, transportation or handling loads during the manufacturing and assembly phase, seismic loads and accidental loads. A description of the loads is given in Table 3.2.

In this Thesis, nominal loads are used to size the system against fatigue. For instance, similar applications registered in a period of 10 years a number of rotations of the gantry

Table 3.2

The expected load scenarios for the supporting system of the cold mass in a superconducting gantry

Scenario	Description
Nominal	Generally, the external varying load, pre-load and cool-down induced stress.
Transportation and handling	The supporting system is subject to extra accelerations every time the cryostat is transported through sites or moved by lifting devices.
Seismic	The supporting system is subject to extra accelerations in the eventuality of earthquakes.
Accidental	The supporting system is subject to accidental loads due to quench.

fatigue cycles equal to $300,000$. Given an estimated life for the system of 30 years, the number of cycles to be expected for the components of the supporting system is about one million. Other loads are used to verify the sizing of the system.

3.5. Formulation of analytical models

As mentioned in Section 3.2 regarding optimization approach, the use of *FEA*s is less favorable, increasing the computational cost of the analysis. The development of analytical solutions is therefore preferred. Additionally, mathematical models developed in this Thesis can help in filling the lack of mathematical formalism in the field. Analytical models formulated in this study must include all necessary boundary conditions and loads to accurately represent real-world conditions and allow the optimization of the supporting architecture. In particular, models must include as input parameters:

- the spatial disposition of all supports;
- the geometry of the single support element;
- the material of the supports;
- the operating temperature.

The minimum output quantities of the model are the stress state of the supports to ensure mechanical resistance and the position (e_x, e_y, e_z) and orientation $(\theta_x, \theta_y, \theta_z)$ of the cryogenic device in order to ensure they are meeting accuracy requirements. In order to study the different loading conditions, the models must include:

- the effect of a generic load composed of forces and moments $\mathbf{F_s} = (F_x, F_y, F_z, M_x, M_y, M_z)$ acting on the cryogenic device;
- the effect of the cool-down or warm-up phases for the cryogenic device;
- the effect of pre-load;
- the effect of the insulation vacuum.

To compare the two architecture types, both the influence of the vacuum vessel stiffness and the stiffness of supports must be included. For the optimization phase alone, the formulation of the models is restricted to the overall geometry of the support architecture, without considering the vacuum vessel influence.

3.6. Comparison analysis metrics

The design methodology chosen foresees that the design candidates are compared against each other through a series of criteria based on the main highlighted requirements.

The compliance with the structural integrity requirement is guaranteed by sizing the supports with the same safety factor on nominal loads. The quantitative comparison parameters are related to the following qualitative factors:

- The compliance with the functionality requirement judged on the basis of the maximum deviation from the nominal position of the cryogenic device. The deviation is compared for each of the six *DOF*s.
- The compliance with the functionality requirement judged on the basis of the heat-flux deposited on from the thermal shield to the cold mass (at 4.7 K) through the supports.
- The compliance with the structural integrity judged on the basis of the safety factor over transportation and handling loads.
- The sensitivity of the system to variations in manufacturing tolerances and pre-load.
- The natural frequencies of the system.

Other qualitative factors are related to the ease of manufacturing, alignment and possible automation of the system.

3.7. IT tools used in the research

The following tools have been used:

- Google scholar for literature analysis;
- Wolfram Mathematica, for solving analytical models, computing, optimizations, sensitivity analysis and 3D figures and plotting;
- Solidworks for 3D modelling;
- *Ansys® Workbench, 2022 R2* for *FEA*s for validation and vibration analysis;
- Microsoft Excel for comparison tables.

4. Main Analyses and Results

This chapter provides an overview of main analysis conducted in Chapters 4–9 of the full Thesis version, highlighting the main results.

4.1. Supporting system architectures and proposed materials

Two supporting systems have been compared in the Thesis: a statically determinate (6S) and indeterminate (8S) configuration. These architectures address the full range of structural possibilities.

The 6S architecture is inspired by the hexapod kinematic design widely used in robotics (Fig. 4.1). Which is worth exploring, since applications of this architecture to cryogenic devices have not been found in literature. This design employs six supports configured as a *6-PSU* or *6-PSS* fully parallel mechanism [58] (see Fig. 4.1 for intuitive understanding of the differences). Prismatic (P) joints at the warm end allow 1D actuation, enabling control of all six *DOF* (degrees of freedom). Spherical (S) or universal (U) joints at the cold end ensure purely axial loading, minimizing internal forces and allowing smaller support cross-sections to reduce heat flux.

The baseline alignment system involves manual adjustment at warm without vacuum, but the architecture could accommodate future automation, which can be highly interesting for active alignment at cold.

The 8S architecture employs the eight-support configuration commonly used for superconducting elements [2], [22], [23], [25], [26], [32], [47]. These supports, featuring spherical or universal joints at both ends (Fig. 4.2) ensure pure internal axial actions transmission in the rods to minimize heat flux.

The 8S architecture represents a good candidate due to its self-aligning behavior, achieved by symmetrically arranging the eight supports. A 3D passive alignment of each warm joint is required to position the cold mass at warm, assisted by an external temporary holding system.

The exclusion of other supporting system candidates and the identification of viable geometries and materials for the supports are discussed extensively in Chapter 4 of the full version of the Thesis. Tubular and double band race track shaped supports are considered. The considered materials are *GFRE* (glass fibre reinforced epoxy), austenitic stainless steel (SS304L), titanium alloy (Ti-6Al-4V), *CFRP* (carbon fibre reinforced polymer) and INVAR.

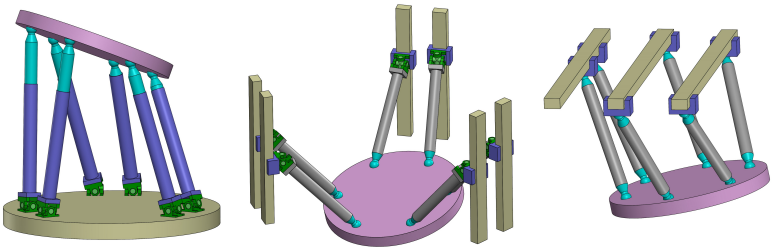

Fig. 4.1. Examples of a common hexapod architectures in robotics. From left to right: 6-UPS, 6-PUS, 6-PSS parallel mechanisms.

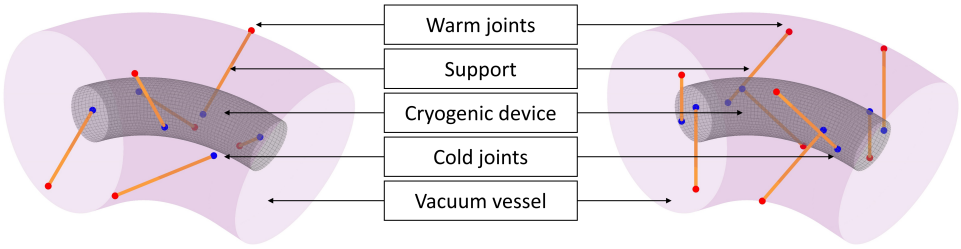

Fig. 4.2. Basic schematic of the 6S (left) and 8S (right) architecture with the cryogenic device (grey), its supports (orange), cold and warm joints (blue and red), and the vacuum vessel (pink).

4.2. Lumped parameter models

The lumped parameter models (*LPMs*) presented in Chapter 5 of the Thesis full version, developed for both statically determinate and indeterminate supporting systems, integrate essential boundary conditions and loads while balancing accuracy and simplicity. These models estimate the pose of the cryogenic device $(e_x, e_y, e_z, \theta_x, \theta_y, \theta_z)$ and the axial internal actions on the supports.

Key mechanical error sources affecting the pose are identified and classified as systematic or random (Table 4.1). Systematic errors are further divided into symmetric and non-symmetric types.

Table 4.1

List and classification of mechanical error sources that contributes to an error in the pose of the cold-mass during operation

Nature	Characteristics	Description
Systematic	Symmetric	Deformation of the support elements
		Deformation of the main structure
		Backlash
	Non-Symmetric	Deformation of the vacuum vessel due to cold-mass weight
		Deformation of the vacuum vessel due to own distributed weight
		Deformation of the vacuum vessel due to differential pressure
		Displacements due to the cool-down process

Random errors, i.e, manufacturing tolerances, alignment and measurement accuracies are analyzed in the sensitivity study (Subsection 4.6.1) to compare the solutions proposed. The requirements in Table 3.1 are related solely to the systematic error budget.

4.2.1. Statically determinate lumped parameter model 6S

The mathematical formalism of the statically determinate *LPM* is built by modifying the *IPK* (inverse position kinematics) and *DPK* (direct position kinematics), two math-

ematical tools from robotics, particularly parallel mechanisms [58]. This section presents the modifications applied to the *IPK* and *DPK* of the hexaglide [59] to account for effects not considered in the original model (i.e, cool-down and vacuum vessel deformation).

The effects on the cold mass position given by the deformation and thermal contraction of supports are introduced in the *IPK* and *DPK* (reported in Thesis Annexes) by modifying the lengths of supports L_i:

$$L_i = (L_{0_i} + \delta_s)\left(1 + \frac{F_{q_i}}{AE}\right), \tag{4.1}$$

where L_{0_i} is the undeformed length at warm, δ_s is the length contraction due to cool-down, E is the Young's modulus of the material, and A is the cross section area of a support. $\mathbf{F}_q$ is the vector of forces on actuated joints, calculated from the force equilibrium with the external forces $\mathbf{F}_s = \mathbf{J}^T\mathbf{F}_q$ ($\mathbf{J}$ is the geometrical Jacobian matrix [60]).

The contribution of the deformation of the vacuum vessl is considered by modifying the *DPK* replacing the target position of the warm joint ${}^0\mathbf{H}_i$ in the *DPK* with a deformed configuration of joints ${}^2\mathbf{H}_i$ calculated as:

$${}^2\mathbf{H}_i = {}^2\mathbf{H}_{0_i} + \boldsymbol{\Delta}_i + q_i\mathbf{h}_i \quad \text{with} \quad \boldsymbol{\Delta}_i = \boldsymbol{\Delta}_{CM_i} + \boldsymbol{\Delta}_{OW_i} + \boldsymbol{\Delta}_{V_i}, \tag{4.2}$$

where the indexes *CM*, *OW*, and *V* are used to differentiate the displacement contributions given respectively by the cold-mass weight, the weight of the vacuum vessel itself, and the differential pressure. A semi-analytic method is used combining measurements from *FEA* to define flexibility tensors of the vacuum vessel, $\mathbf{D}_{CM}$ and $\mathbf{D}_{OW}$. This method gives the possibility of checking the contribution of the vacuum vessel to the pose error for a generic external load, running only six initial *FEA* (one analysis for each support). The constant contribution of pressure $\boldsymbol{\Delta}_{V_i}$ is directly measured from *FEA*. The practical procedure to get $\mathbf{D}_{CM}$ and $\mathbf{D}_{OW}$ is explained explicitly in Chapter 5 of the Thesis and in an article published [61].

The contribution of backlash in the joints is also added in the *DPK* by modifying the real position of the joints (${}^{2,1}\mathbf{M}_{r_i}$ or ${}^2\mathbf{H}_{r_i}$):

$${}^{2,1}\mathbf{M}_{r_i} = \begin{cases} {}^{2,1}\mathbf{M}_{\text{nom}_i} - \frac{b_c}{2}\mathbf{w}_i & \text{if} \quad F_{q_i} > 0 \\ {}^{2,1}\mathbf{M}_{\text{nom}_i} + \frac{b_c}{2}\mathbf{w}_i & \text{if} \quad F_{q_i} < 0 \end{cases}, \tag{4.3}$$

$${}^2\mathbf{H}_{r_i} = \begin{cases} {}^2\mathbf{H}_{\text{nom}_i} + \frac{b_h}{2}\mathbf{w}_i & \text{if} \quad F_{q_i} > 0 \\ {}^2\mathbf{H}_{\text{nom}_i} - \frac{b_h}{2}\mathbf{w}_i & \text{if} \quad F_{q_i} < 0 \end{cases}, \tag{4.4}$$

where, ${}^{2,1}\mathbf{M}_{\text{nom}_i}$ and ${}^2\mathbf{H}_{\text{nom}_i}$ are the nominal joints; b_c and b_h are the values of backlash (radial internal clearance), respectively, of cold and warm joints and $\mathbf{w}_i$ gives the direction of the nominal support element.

4.2.2. Statically indeterminate general lumped parameter model

For statically indeterminate supporting systems of cryogenic devices, applying *DPK* is not feasible, as it relies on a purely geometric solution. While the *LPM* for solution 6S introduces modifications in the form of deformations or contractions of the supports, these remain independent among supports. In the statically determinate case, the bodies behave as shortened versions displaced only by rigid body motion.

Conversely, in a *LPM* for a statically indeterminate system, the stress and deformation of each support depend on the state of all others. Therefore, a generic model based on the energy-based principle of virtual work [62], [63], applicable to any configuration with

more than six linking bar supports ($n > 6$), is developed. The complete mathematical derivation is discussed in the full text of the Thesis and has been published in [64]

The principle of virtual work applied to over-constrained structures requires to find a compatible exactly-constrained structure where enough constraints are substituted with an equal number of variables. A total of $n-6$ X_m variables are introduced to eliminate the $n-6$ extra constraints resulting in the compatible structure represented in Fig. 4.3.

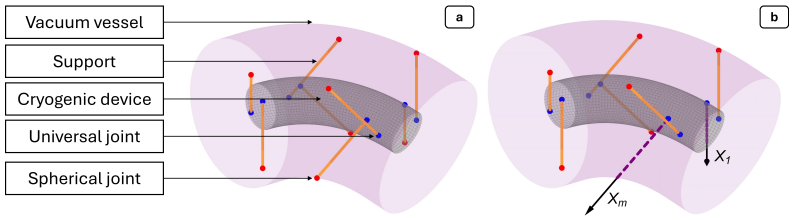

Fig. 4.3. **a)** Cryogenic device (gray) supported by eight supports (orange) joined to it by mean of universal joints (blue) and to the vacuum vessel (pink) by mean of spherical joints (red). **b)** Compatible exactly constrained structure with over-constrained variables $X_1, ..., X_m$. In purple the supports where constraints have been substituted with over-constrained variables.

The principle of virtual work requires to find the internal actions for $n-5$ cases of the compatible structure, as clarified in the following list:

- one compatible structure where only external loads are applied, used to calculate $\mathbf{N}_0$ – the vector containing internal actions on each support.
- $n-6$ compatible structures where the over-constrained variables X_m are applied one by one as unitary loads, used to calculate $\mathbf{N}_{X_m}$ – the vector containing the internal actions on each support.

A system of $n-6$ equations must be written to calculate all $n-6$ over-constrained variables X_m, each equation in the form of Equation (4.5).

$$\sum_{i=1}^{n} \int_0^{L_i} N_{X_{mi}} \left(\frac{N_{0i} + \sum_{p=1}^{n-6} X_p N_{X_{pi}}}{E_i A_i} + \frac{\delta_i}{L_i} - \frac{\delta_{P_i}}{L_i} \right) ds = \mathcal{W}_{\text{ext}_{X_m}} , \tag{4.5}$$

where δ and δ_P add the contributions respectively of the thermal differential contraction or expansion and the pre-load in terms of length adjustment. Additionally, each support is described by a unique length L_i, cross section A_i and material Young modulus E_i.

The thermal differential contraction or expansion; axial actions due to over-constrained variables $N_{X_{mi}}$, external loads N_{0i}, and contributions to the work done by external reactions $\mathcal{W}_{\text{ext}_{X_m}}$ depending on warm joints displacement $\mathbf{\Delta}_i$, such as the deformation of the vacuum vessel, are formally defined in Chapter 5 of the Thesis.

Once all X_m are known, the principle of virtual work can be applied again to extract the pose (position and rotation) $\mathbf{e} = (e_x, e_y, e_z, \theta_x, \theta_y, \theta_z)$ of the cryogenic device by solving six independent equations in the form of Equation (4.6). Each equation requires to calculate the internal actions $\mathbf{N}_j$ on each support when an unitary force/torque is applied to the compatible structure.

$$\sum_{i=1}^{n} \int_0^{L_i} N_{ji} \left(\frac{N_{0i} + \sum_{p=1}^{n-6} X_p N_{X_{pi}}}{E_i A_i} + \frac{\delta_i}{L_i} - \frac{\delta_{P_i}}{L_i} \right) ds = \mathbf{d} \cdot \mathbf{N}_j + e_j = \mathcal{W}_{\text{ext}_j} , \tag{4.6}$$

where the internal actions $\mathbf{N}_j$ and the displacements $\mathbf{d}$ are formally defined in the full text version of the Thesis.

4.3. Validation of the lumped parameter models

The models developed in Section 4.2 have been validated by comparing their results with thermo-mechanical simulations obtained from a widely used *FEA* software(*Ansys® Workbench, 2022 R2*). The validation of both models developed in this study has been conducted separately and is reported in Chapter 6 of the Thesis.

The validation of the *LPM*s is first conducted on the generic statically indeterminate support configuration using eight and eleven-support geometries.

The validation of the 6S *LPM* is conducted in the gantry case study. An initial benchmark assesses the effects of gravity, pre-load, temperature, and pressure on the magnet's pose during gantry rotation, followed by a second benchmark validating the model's treatment of backlash.

For the 8S *LPM* applied to the gantry study case, a validation is performed with the same methodology as the 6S case to the gantry study.

4.3.1. Overall validation methodology

A series of linear static steady-state thermo-mechanical *FEA*s were performed. The main simulation parameters are provided in the following paragraphs, while specific assumptions for each case are discussed only in the full Thesis version.

- **Geometry**: The simulations of the generic model statically indeterminate model use respectively a generic asymmetric eight and eleven support configuration. The validation of the 6S and 8S gantry solutions use the optimized geometry from later-stage routines (Section 4.4) associated to the first cold mass of the gantry transfer line. Each support connects to the vacuum vessel via a spherical joint and to the cold mass via a universal joint. For validation, no thermalization is applied to split supports.
- **Material**: Temperature-dependent coefficient of thermal expansion and thermal conductivity of stainless steel 304 [65] are being used to define the properties of the steel material applied to supporting elements.
- **Interactions**: Spherical joints and bushing joints (general Ansys joint defined by stiffness parameters) have been used to simulate the joints between the supports and the vacuum vessel or supports and cold-mass. Bushings are used to formulate an universal joint between the nodes by defining the stiffness associated with the degrees of freedom to lock.
- **Loads**: The first step simulates the cold mass behavior during cool-down, lowering its temperature from 22 °C to −268 °C without additional loads. Pre-load and vacuum pressure are applied in subsequent steps. The external load is introduced later, either representing the magnet's weight for gantry-related validations or a generic load for the *LPM* validation, in Subsection 4.3.2.

4.3.2. Validation of the generic over-constrained LPM

The geometry of this benchmarking has been randomly generated for the 11-support configuration to prove that the mathematical model developed can be adapted to non-symmetrical configurations too. The 8-support configuration is the same as the 11-support where three supports have been suppressed.

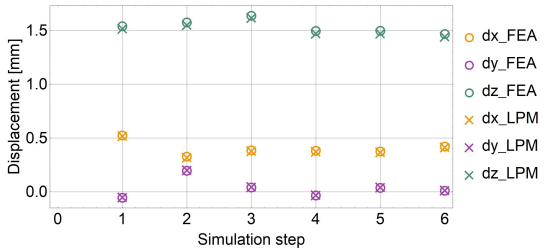

Fig. 4.4. Comparison of the pose (displacement and rotation) of the cold-mass between the *LPM* (cross) and *FEA* (circle). Complete picture for both 8 and 11 supports is presented in the full text.

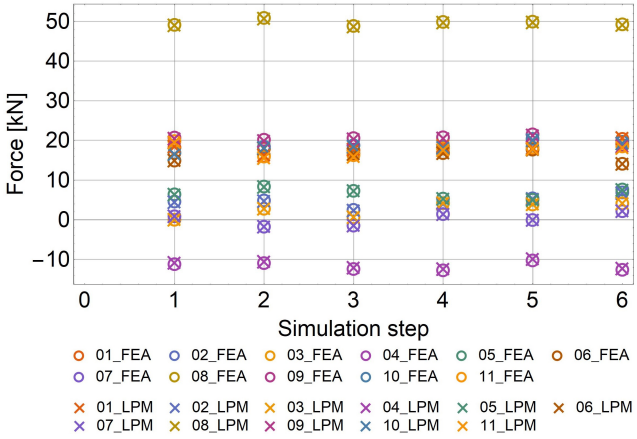

Fig. 4.5. Comparison of the force on each support between the *LPM* (cross) and *FEA* (circle). Complete picture for both 8 and 11 supports in the full text.

The agreement with the *LPM* is shown in Fig. 4.4. Detailed tables reporting the values of all pose components are found in the full text version. Even though some high errors appear in particular cases, the median of all errors is only about 0.6 % and 1.4 %, respectively for the eight-support and eleven-support study cases, confirming for the pose a very good agreement of the developed model with *FEA*s. The accuracy slightly decreases for the model with eleven supports but is still accurate enough to be used in optimization processes, the comparison of different material and dimensional solutions, and sensitivity analysis.

Values of internal axial load on each support for each loading case simulated with *FEA* are reported in tables in Capter 6 of the Thesis. The median relative errors are about 1.1 % and 1.4 % respectively for the eight-support and eleven-support study case. This quantitatively confirms the very good agreement of the model with *FEA*s. Although the accuracy slightly decreases with a larger number of rods, the model can be judged reliable.

The validation highlights the ability of the model to correctly estimate interesting quantities, such as loads and position of objects, in a general way. The validation proves the effectiveness of the model in predicting those quantities, even for support configurations that are highly non-symmetrical.

Computational performance and system details are provided in the full text of the

Thesis for result reproducibility. Both *LPM* and *FEA* simulations were run on the same machine using Wolfram Mathematica and Ansys, respectively. The *LPM* achieves a 20-fold speed improvement over widely used *FEA* software.

While a single *FEA* simulation takes 25 s, making the *LPM* seem unnecessary for isolated cases, its efficiency greatly benefits optimization algorithms. For instance, analyzing 100,000 configurations of an 11-support system would take 1.4 days with the *LPM*, compared to 29 days using *FEA*. Additionally, the mathematical model serves as a valuable cross-check for *FEA* results, which are highly sensitive to simulation settings and boundary conditions.

4.3.3. Validation of the LPM for 6S applied to the gantry study case

Results of the validation of the 6S *LPM* applied to the gantry study case are reported in Fig. 4.6 for the benchmarking of the pose, and in Fig. 4.7, for the axial actions in the supports. A very good correlation between the *LPM* and *FEA* has been found. Tables with the numerical values associated to the plots presented can be found in the full text version of the Thesis.

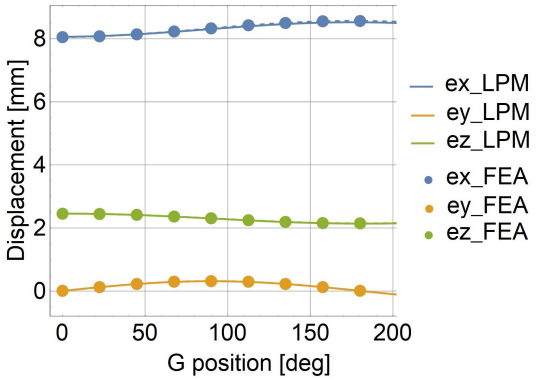

Fig. 4.6. Evolution of the pose $(e_x, e_y, e_z, \theta_x, \theta_y, \theta_z)$ during the rotation of the gantry as calculated from *LPM* (continuous lines) and from *FEA*s (points and dotted lines). Rotation results are shown in the Thesis full text.

Overall, the absolute disagreements are at least one order of magnitude smaller than the accuracy required to the application. Hence the model is proven perfectly suitable for comparative studies, optimization studies, and sensitivity studies. For alignment campaigns, without additional experimental testing, the models are considered at least as accurate as *FEA*s in providing initial values for the alignment.

Additional structural mechanics *FEA* have been conducted to validate the backlash effect formulated in the 6S *LPM*. The backlash in the spherical joints has been simulated by introducing three longitudinal springs (one for each transnational *DOF*) between the rod end bearing and the rod end body.

Results of the *FEA*s to validate the backlash behavior are reported in Fig. 4.8. Few mismatches between *LPM* and *FEA* have been found at around 50° and 230°, which are points at which the reaction force on one of the supports happens to be almost zero (better discussed in the full text version). Thus, just in this interval, the non linear springs elongate less than the value of backlash, generating unreliable results from the *FEA* side. In conclusion, the modification to the *DPK* described for the *LPM* are proven effective

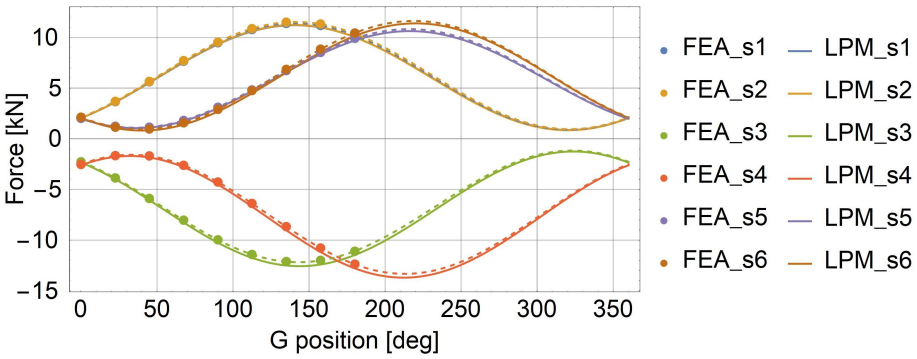

Fig. 4.7. Internal actions on all six supports of solution 6S: *LPM* results (continuous lines), *FEA* results (points), *FEA* fitted curves (dashed lines).

in estimating the pose of the cold-mass during a rotation of the gantry if joints present backlash.

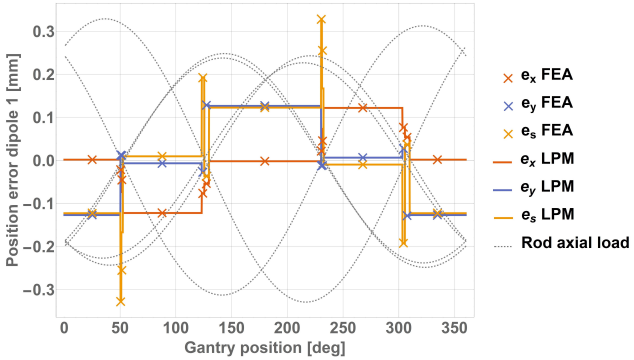

Fig. 4.8. Position and rotation errors due to backlash. Continuous lines show results as calculated from the *LPM*, points are values obtained by structural *FEA*. Rotation results are shown in the Thesis full text.

4.3.4. Validation of the 8S LPM applied to the gantry study case

The *LPM* for over constrained supporting systems has been particularized to the study case of the gantry. This benchmark follows the same methodology used in Subsection 4.3.3. The materials used, loads applied and boundary conditions of the model are explained in detail in the full version of the Thesis.

Results of pose and axial internal actions for a series of positions of the gantry are shown in the plots in Fig. 4.9 and Fig. 4.10, points show the results of *FEA*s. The absolute values of the disagreement between the two models are much lower than the usual range of accuracy required for these machines (see Table 3.1).

The average force differs, in the worst case, by 0.73 kN between *LPM* and *FEA*, which is about 0.83 % on the average force of 87 kN measured from *FEA*s. The force amplitudes differ, in the worst case, by 24.6 N or 0.77 % in relative terms. These values confirm a good accuracy of the *LPM* model, with respect to standard simulation methods, to predict

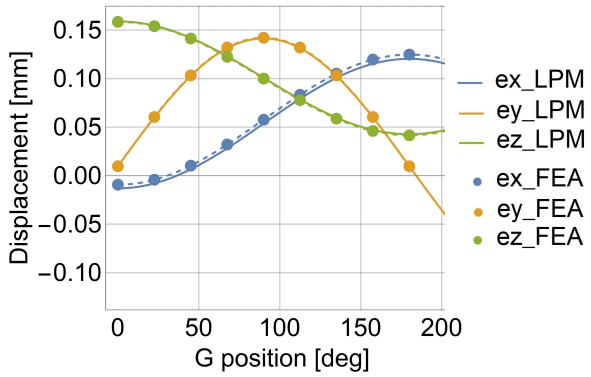

Fig. 4.9. Comparison of the pose (displacement and rotation) of the cold-mass between the *LPM* (continuous lines) and *FEA* (points). Rotation results are shown in the Thesis full text.

forces for an over-constrained architecture. Given their proven accuracy in estimating both pose of the device and the loads on the supports, the developed models are considered applicable to the over-constrained study case.

4.3.5. Conclusions on the validation

To conclude, the models of an exactly constrained supporting system and an over-constrained supporting system have been validated against *Ansys* 2022. The results show that the developed models are in good agreement with *FEA* results. An important achievement in the validation process has been the validation of the generic formulation of the *LPM*, model that can be used for supporting systems with many supporting rods (≥ 6), arranged in a configuration that may be not necessarily symmetric, and dimensions and material can be different for each rod. These studies estimate an agreement between *FEA*s and the developed *LPM* of 99.4 % and 98.6 % (calculated on simulations of 8 and 11-support configurations). The developed code based on *LPM*s outperformed *FEA*s by around 20 times in computing time, as demonstrated in Section 6.2 of the Thesis. Additionally, the use of the developed *LPM*, which is much simpler than *FEA* in the number of parameters needed to set up a simulation, can establish a more insightful overview of the mechanical response of a complex system, allowing designers and analysts to have a clearer grasp on the relationships between the results and the most relevant input quantities. In contrast, *FEA*s, based on a large number of options and input parameters, require extensive studies to map the relationship between relevant input parameters and output quantities, with a great dependence on the experience of the user and the correct settings of the many options. All above mentioned results make the developed model interesting also for other cryogenic applications different from the medical application studied in this research, such as radio frequency superconducting cavities, optical positioning systems at cold, satellites, superconducting generators or motors.

The models agree with *FEA* results with an accuracy of 97 % and 98.5 % for the 6S and 8S gantry solutions, respectively. Overall, even when relative agreement is higher than the average value, absolute agreement is at least one order of magnitude smaller than the required accuracy for the application. Consequently, the models developed are completely adequate for comparative analysis of materials, dimensions, etc... Considering the computational advantage the codes can give, the disagreement of 1.5–3 % becomes

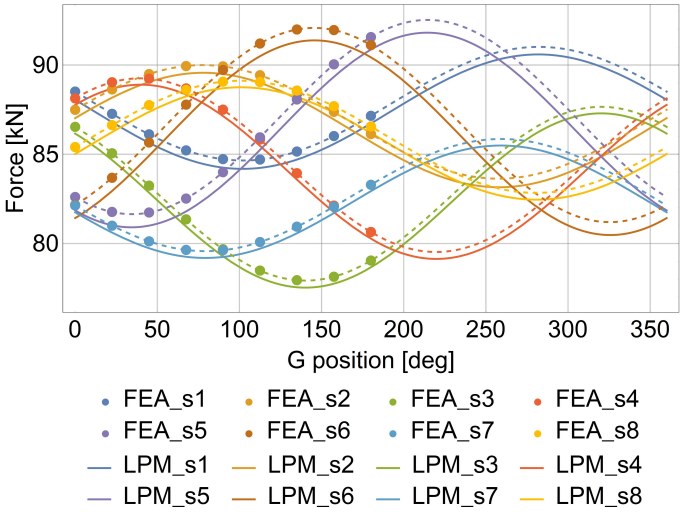

Fig. 4.10. Comparison of the force on each support in the *LPM* (continuous lines) and *FEA* (points).

even less significant if the models are used for optimization routines or sensitivity analysis where a large number of configurations must be checked, as it will be done in this Thesis in following chapters.

4.4. Optimization

The choice of the arrangement of each of the supports and of the geometry (rod or double band) and material of supports influences crucial parameters and must be subject of optimization in order to:

- maximize system rigidity throughout the entire rotation, not just at a single working position;
- distribute loads evenly across supports, enabling smaller cross-sections and minimizing heat loads;
- enable full backlash recovery with minimal pre-load, reducing loads and heat loads on the supports;
- minimize extra-loads during cool-down for the over-constrained solution.

Each support in the proposed systems (shown in Fig. 4.2) is defined by five parameters: three for the cold joint position, $\mathbf{M_i} = (M_{xi}, M_{yi}, M_{zi})$, and two angles, α_1 and α_2, for its axial direction. This results in 30 and 40 variables for the two systems. Applying symmetry and accounting for the self-aligning nature of the over-constrained system reduces the parameters to 16 (determinate) and 6 (indeterminate), respectively.

Due to the high number of variables and constraints, such as those ensuring manufacturability of the cryostat, a *GA* (genetic algorithm) [66] is employed, its implementation is discussed in Chapter 7 of the Thesis. *GA*s are biologically inspired algorithms based on four main steps, in order: initialization, evaluation, selection, and genetic recombination. *GA*s tend to converge quickly to local optima. To promote exploration and avoid premature convergence, this study uses the "island model" *GA* [67], a parallel approach that improves diversity. The fitness function includes only the part of the *LPM*s related

to cold mass displacement due to support deformation. The vacuum vessel geometry is excluded from the optimization, as its stiffness can be increased with negligible effects on heat loads and overall machine weight.

The performance of each individual is quantified defining a scalar value or "fitness". The fitness is a figure of merit related to the overall pose $(e_x, e_y, e_z, \theta_x, \theta_y, \theta_z)$ (position and rotation) limited to the deformation of supports. The raw fitness is calculated by

$$f = \frac{1}{\sqrt{\mathbf{P_e} \cdot \mathbf{P_e}}} \quad \text{with} \quad \mathbf{P_e} = (\tilde{e_1}, \cdots, \tilde{e_6}) \,, \tag{4.7}$$

where $\tilde{e}_i$ is the max error during a load cycle (rotation of the gantry). A larger value of f characterizes an individual that shows overall less pose error than another. Penalty functions have been applied to the raw fitness to account for the efficacy of the pre-load system (p_1) and to minimize the loads on the supports (p_2). Applying the mentioned penalty functions (explained in detail in Chapter 7 of the Thesis), to Equation (4.7), the final fitness function is:

$$\tilde{f} = f p_1 p_2 \,, \tag{4.8}$$

The overall developed routine is illustrated in Fig. 4.11.

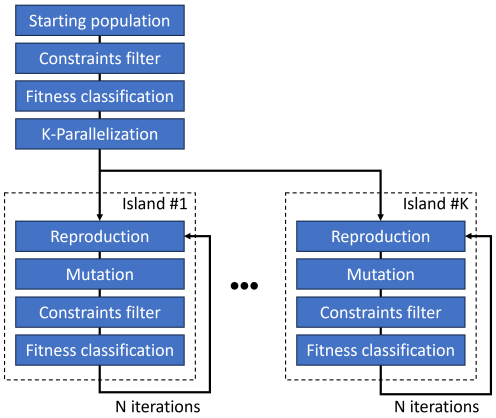

Fig. 4.11. Flowchart of the genetic algorithm used in this Thesis.

The steps are here summarized:

1. A starting population of n individuals gets randomly generated.
2. Constrains are applied to the population to filter for valid individuals.
3. The fitness of the individuals of the starting population is evaluated, and individuals are classified accordingly.
4. The first k individuals of the starting population become the first generation elites and are separated into k islands.
5. The population of the island reproduces by mitosis, copying the support arrangement of the elite.
6. The population of the island is subject to random mutations.
7. Constrains are applied to the population of the island to filter for valid individuals.
8. The fitness of the individuals of the starting population is evaluated, and individuals are classified accordingly.

Additional rules are imposed to the algorithm:

- Steps 5–8 for each island happen in parallel.
- The most fit individual of an island is added to the next iteration of the same island to preserve the performances of that island.
- No cross-island interaction is programmed, no new islands are generated. Both measures are put in place to avoid genetic diversity loss.
- At the end of each iteration, the fitness values of all islands are compared to adapt the mutation strategy. Islands with lower maximum fitness undergo more intense mutation and affect a larger number of individuals, promoting exploration of the solution space. In contrast, islands with higher maximum fitness are used for exploitation and are mutated less.

4.5. Design of the supporting systems: The gantry case study

This section presents the final design choices for both supporting systems (6S and 8S). It begins by highlighting the advantages of the proposed support arrangement optimization strategy, applied consistently to both solutions, though results are shown only for 6S, following the routine in Section 4.4. Next, the *LPM*s are used to compare different materials and support cross-sections, aiming to minimize heat loads while ensuring sufficient stiffness to meet accuracy requirements. Additional design aspects, including the use of a pre-load backlash removal system and the alignment system design, are also discussed.

4.5.1. 6S optimization results

Two comparative analyses were conducted to demonstrate the effectiveness of the optimization routine and the benefits of a backlash recovery system. The first compares solution S1 (original, un-optimized system) with solution S2 (optimized system). The second compares solution S3 (optimized system with backlash) to solution S4 (optimized system with pre-load).

Pose accuracy improved by an average of 16 % between S1 and S2, with the most significant improvement seen in θ_x, which improved by 83 %. This was particularly important, as the initial value of 0.6 mrad in S1 was already at the limit of the requirements (Table 3.1). A notable improvement is also observed in e_y, which decreased by 45 %, from 0.27 mm to 0.15 mm. Although e_x deteriorated by 87 %, this is considered acceptable since beam performance is less sensitive to longitudinal errors, and difference is the outcome of design choices that were not considered in the initial design of the vacuum vessel. Plots of all pose components for S1 and S2 are available in Annexes of the Thesis.

Thanks to the introduction of penalty functions in the fitness function $\tilde{\mathbf{f}}$, thermal insulation capabilities are also improved. As a direct consequence of the optimization, a decrease of the required pre-load is reached lowering the reaction load on each support by 44 %, consequently lowering the required cross-section to achieve the same safety factor. Hence a proportional reduction by 44 % of the conductive heat-load to the cold-mass has been achieved. The power required to extract this heat at 4.7 K using cryocoolers (with the *SHI RDK-415D2 4K* as an example) is around 2.6 kW, leading to a reduction of approximately 2.2 kW in the required power.

The optimization routine proposed in this study demonstrates useful also to extrapolate conclusions on basic design choices. After running the algorithm for 10 times, the results seem to converge in moving two initially non-symmetric supports in a symmetric manner, as illustrated in Fig. 4.12.

Table 4.2

Absolute errors and percentile improvement for each *DOF* for an initial support configuration and the optimized one

DOF	Initial (S1)	Optimized (S2)		Improvement
$\mathbf{e_x}$	0.18	0.34	mm	−87 %
$\mathbf{e_y}$	0.27	0.15	mm	45 %
$\mathbf{e_z}$	0.20	0.19	mm	3 %
$\theta_\mathbf{x}$	0.60	0.10	mrad	83 %
$\theta_\mathbf{y}$	0.10	0.05	mrad	55 %
$\theta_\mathbf{z}$	0.07	0.07	mrad	−1 %
$\mathbf{f}$	(3.1, 1.6, 2.0, 2.0)	(4.3, 5.2, 4.8, 2.7)		
$\tilde{\mathbf{f}}$	$(\approx 0, \approx 0, \approx 0, \approx 0)$	(4.3, 5.2, 4.8, 1.2)		
$\mathbf{F_{q,max}}$	35.5	19.8	kN	44 %
bulk diameter	24	18	mm	
safety factor	12	12.2		
heat-load @ 4.7 K	1	0.55	W	44 %
compressor input power	4.8	2.6	kW	44 %

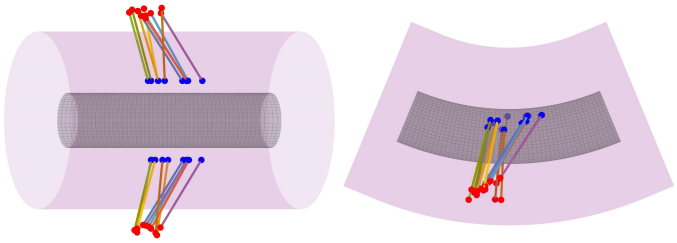

Fig. 4.12. Position of the initially non-symmetric supports after 10 runs of the genetic algorithm. Only the supports left initially unconstrained by symmetry are shown.

4.5.2. 6S backlash and pre-load system

This section compares solution S3, which allows backlash in the joints, with S4, which compensates for it through pre-load and higher loads. Pre-loading shifts the axial reactions so that each support remains either always in tension or in compression, ensuring the joints stay in the same position throughout gantry rotation (Fig. 4.13). This reduces the error on the alignment of magnets and therefore increases the beam performances (Fig. 4.14).

The plots in Fig. 4.14 focus on the *DOF* with the greatest improvement (all other plots are available in the full version of the Thesis). A summary of the results is shown in Table 4.3. Five *DOF*s improved by 46–71 %, while the error on θ_x shows only a minor decrease in accuracy. The added pre-load increases the loads on the supports, doubling the conduction heat load to the cold mass-from approximately 0.25 W to 0.55 W at 4.7 K-cumulatively across all six supports. Despite a 120 % increase in heat load, the pre-load system and optimized geometry keep pose variations during rotation within the required limits, demonstrating its efficacy.

4.5.3. 6S material and dimensions choice

In the next design phase, the baseline material and dimensions of the supports are selected by evaluating three figures of merit: structural integrity (Fig. 4.15), based on the safety factor under nominal static loads; operational accuracy (Fig. 4.15), the main functionality criterion, based on Equation (4.7), with the addition of vacuum vessel deforma-

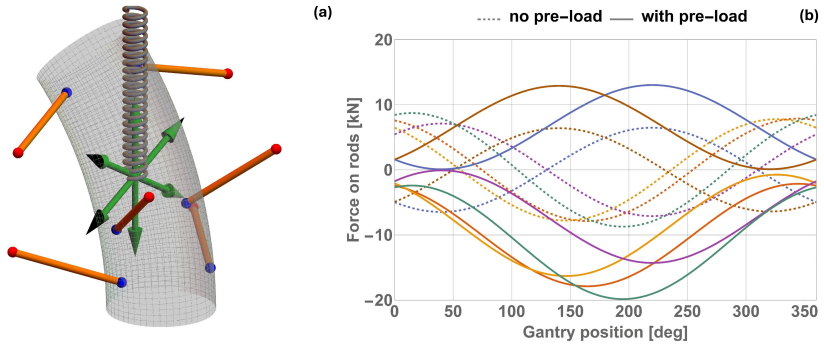

Fig. 4.13. (**a**) Conceptual scheme of the pre-load represented by the spring and gravity load (in green) during the rotation of the gantry. (**b**) Effect of pre-load on rods internal actions in relation to the gantry position.

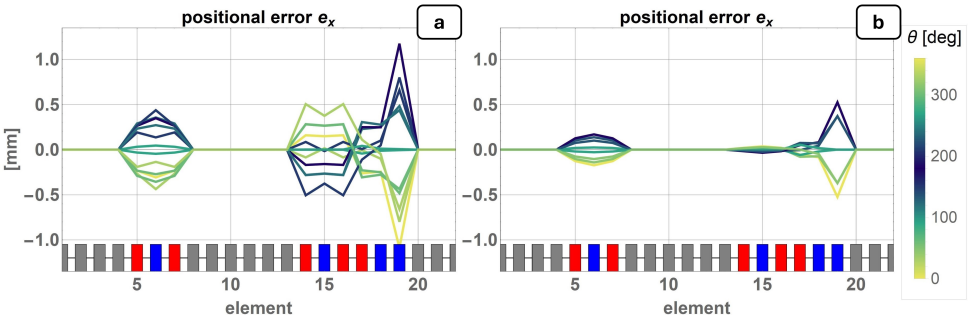

Fig. 4.14. (**a**) Results of position error e_x in S3. (**b**) Results of position error e_x in S4. Rotation results are shown in the Thesis full text.

tion contribution; conductive heat-load (Fig. 4.16), calculated using thermal conductivity integrals [65], [68], assuming thermalization at the support midpoint.

The support sizing and material selection are based on a minimum safety factor of 12, chosen to account for high-cycle fatigue. The figures of merit versus equivalent diameter are shown in Fig. 4.15 and Fig. 4.16. The distinct curves per material in Fig. 4.15 reflect different loading conditions of the cryostat modules along the transfer line. The pose figure of merit ranges from 2 (titanium) to 2.8 (stainless steel), indicating that stainless steel would be preferable solely from a pose accuracy standpoint. However, titanium supports conduct significantly less heat from 60 K to 4.7 K for any diameter (Fig. 4.16). Thus, Ti6Al4V is selected as the baseline material, offering the best trade-off across all figures of merit.

4.5.4. 6S mechanical design

This subsection describes the technical integration of selected arrangement, size and geometry of supports into the cryostat, aiming to assess the feasibility and manufacturability of the design. Six tubular Ti6Al4V supports suspend the cold mass (Fig. 4.17). A high thermal conductivity material is placed at the mid-length of each support to intercept the conductive heat-flux at an intermediate temperature. Spherical joints at both ends prevent over-constraint, while a prismatic joint (linear guide) at the warm end, actuated

Table 4.3

Absolute errors and percentile improvement for each *DOF* for the comparison of S3 with S4

DOF	With backlash (S3)	With pre-load (S4)		Improvement
$\mathbf{e_x}$	1.18	0.52	mm	55 %
$\mathbf{e_y}$	0.67	0.33	mm	52 %
$\mathbf{e_z}$	0.93	0.39	mm	59 %
$\theta_\mathbf{x}$	0.50	0.54	mrad	−8 %
$\theta_\mathbf{y}$	0.57	0.16	mrad	71 %
$\theta_\mathbf{z}$	0.31	0.17	mrad	46 %
$\mathbf{F_{q,max}}$	8.7	19.8	kN	-130 %
bulk diameter	12	18	mm	
safety factor	12	12.2		
heat-load @ 4.7 K	0.25	0.55	W	-120 %
compressor input power	1.2	2.6	kW	-120 %

Table 4.4

List of material properties for the compared materials for solution 6S and 8S

	Ti6Al4V	SS304L	Invar 36	CFRP	GFRE	
Yeld strength	950	205	483	2000	300	MPa
Young's modulus	114	195	148	130	30	GPa

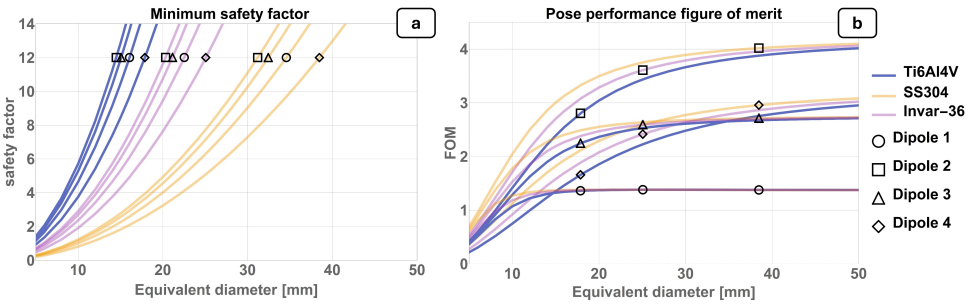

Fig. 4.15. Relation of safety factor (**a**) and pose performance (**b**) on dimensions and material for the statically determinate solution.

by a lead screw mechanism, enables independent motion of the six warm joints. This actuation allows full control of the cold mass position across all six degrees of freedom.

The alignment range is defined based on an assessment of potential cold mass misalignments arising from assembly and manufacturing tolerances using Monte Carlo simulations. From this, the maximum required travel of warm joints to correct misalignments was determined. A lead-screw assembly was designed to provide the necessary linear motion. Torque-multiplying wrenches (with ratios between 1 : 5 and 1 : 25) are needed to manually operate the lead-screws. This improves the alignment precision which results approximately 0.05 mm and 0.05 mrad at 3σ. The integration of a pneumatic pre-load system, powered by standard pressurized lines, is essential to eliminate accuracy losses due to joint backlash, as discussed in Subsection 4.5.2.

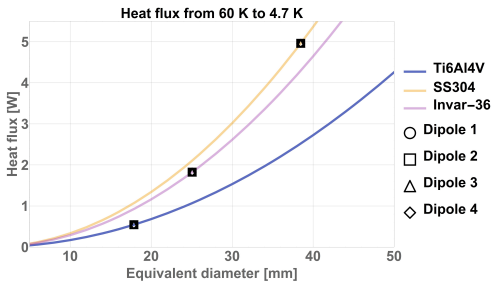

Fig. 4.16. Dependence of heat load to 4.7 K on dimensions and material for the statically determinate solution.

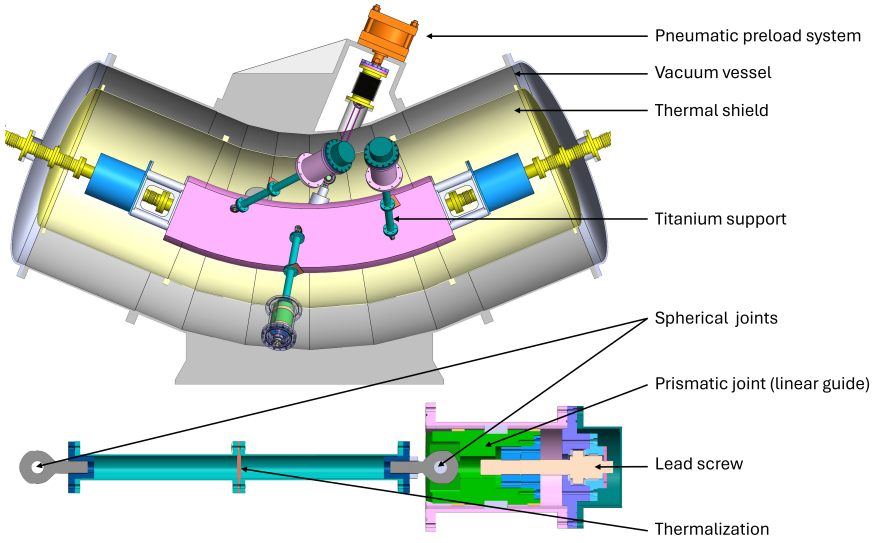

Fig. 4.17. 3D model showing the main components of the parallel supporting system.

4.5.5. 8S Material and dimensions choice

The support arrangement for the 8S architecture is optimized using the algorithm described in Section 4.4 for the 6S system. The only change lies in the *LPM* used to compute the magnet pose. A key difference in assumptions is that backlash is mitigated by applying sufficient pre-load at the warm end to all supports simultaneously, instead of using a pneumatic system.

After optimizing the support arrangement, the baseline material and dimensions were selected using the same three figures of merit as for the 6S solution: safety factor under static loads, operational accuracy, and conductive heat-load through the supports. Results are shown in Fig. 4.18 and Fig. 4.19. In contrast with the 6S supporting system, where the load doesn't depend on the elastic modulus of material, for the over-constrained architecture 8S, the load depends on the stiffness of the support and also on the effect of differential thermal contractions. The dipole in the most critical condition does depend on the material chosen, unlike solution 6S.

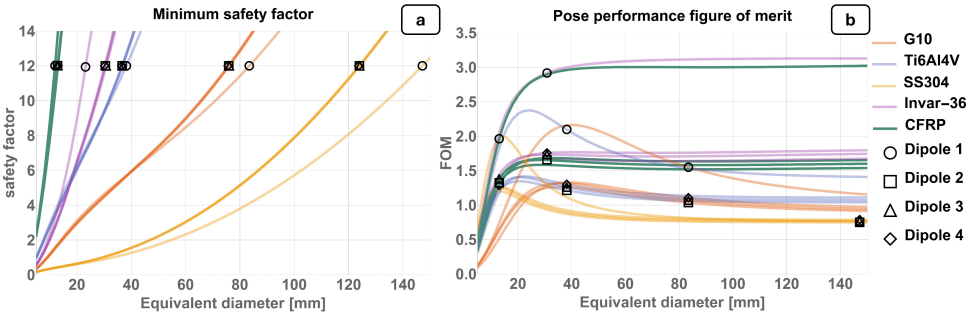

Fig. 4.18. Dependence of safety factor (**a**) and pose performance (**b**) on dimensions and material for the statically indeterminate solution.

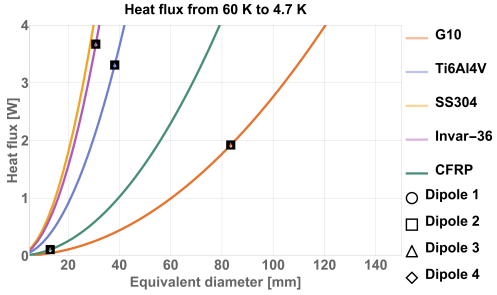

Fig. 4.19. Dependence of heat load to 4.7 K on dimensions and material for the statically determinate solution.

Given the results, all solutions satisfy the minimum safety factor coefficient required (12). The figure of merit for the rigidity of the system ranges between 0.77 to 2.02, respectively, for SS304 and Invar-36. Support solutions in SS304 and *GFRE* are deemed critical, having lower pose performances, while other solutions are still good candidates. The solution in *CFRP* outperforms by 17 times the second best solution in terms of heat flux to 4.7 K, therefore, it has been chosen as baseline for the 8S supporting system design.

4.5.6. 8S mechanical design

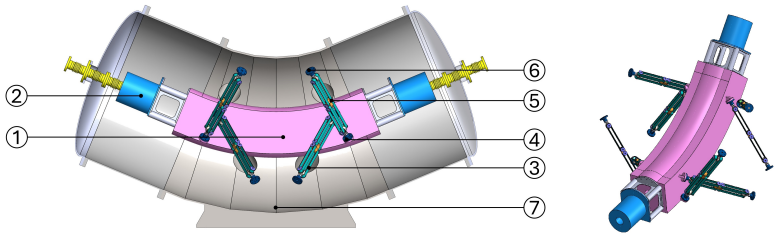

Fig. 4.20. 3D model of the support architecture: 1– superconducting dipole; 2– superconducting quadrupole; 3– support; 4– cold joint; 5– thermalization; 6– warm joint with 3D alignement system; 7– vacuum vessel.

The support system shown in Fig. 4.20 adopts a double-band design for the supporting elements (Fig. 4.21). The band geometry allows for uni-directional fiber layup, maximizing strength while minimizing shear stress concentration and delamination risks. A clear advantage of the double-band design over tubular composite rods is seen at the thermalization, which should ideally divide the support into two segments. In a rod-based design, this would require mechanical or adhesive joints, both vulnerable to failure under repeated thermal cycling. The double-band geometry, as illustrated in Fig. 4.21, resolves this by permitting the composite material to contract freely.

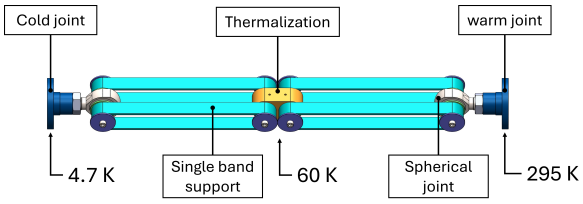

Fig. 4.21. Proposed over-constrained support sub-assembly: cold joint at 4.7 K, (2) single band shaped support, thermalization, rod end, warm joint at 295 K.

A possible alignment strategy for solution 8S is here proposed:

1. The position of the cold mass at room temperature is assumed as nominal, the misalignment of the position of the cold mass at operating temperature is calculated by mean of the *LPM*.
2. The target position of the cold mass at room temperature is shifted accordingly to the misalignments calculated at step 1.
3. The cold mass is positioned within the vacuum vessel at the target position (step 2) at the best of the position measurements uncertainty of an external positioning stand.
4. The eight supports are connected to a warm joint 3D positioning system.
5. Minimum pre-load is applied to recover backlash, internal load is monitored.
6. The external positioning stand is removed.
7. Full pre-load is applied.

A potential limitation of this procedure lies in the need to align the cold mass using an external positioning stand, an operation more easily performed on the ground than

directly on the machine. First, the reference system of each cryostat must be located relative to the machine's reference frame to account for gantry manufacturing tolerances. Then, the cryostat is lowered to the ground, and the cold mass is aligned using the external positioning stand, which must itself include alignment capabilities. Finally, the fully assembled cryostat, with the cold mass in position, is installed onto the machine.

4.6. Comparative analysis of the supporting systems in the gantry study case

This chapter compares the optimized versions of the exactly constrained (6S) and over-constrained (8S) supporting systems. The comparison is based on the following figures of merit:

- Accuracy– maximum pose error along the beam transfer line for all cold elements, evaluated for each *DOF*.
- Nominal structural integrity– safety factor under static nominal loads.
- Conductive heat-flux from the thermal shield to the cold mass through the supports.
- Sensitivity– standard deviation of the cryogenic device pose due to variations in geometry and material properties.
- Structural integrity under handling– safety factor under transportation and handling loads (assumed static).
- Dynamic behavior– comparison of the natural frequencies of both solutions.

The accuracy, nominal structural integrity, and heat-flux figures of merit are summarized in Table 4.5, while the remaining comparisons are addressed in the following sections.

Table 4.5

Comparison of the first three figures of merit for solution 6S and 8S

		6S	**8S**	**% improv.**
Material		Ti6Al4V	CFRP	
Geometry		tube	double band	
Equivalent diameter	mm	18.0	13.2	
e_x	mm	0.36	0.37	−4 %
e_y	mm	0.32	0.24	23 %
e_s	mm	0.45	0.36	20 %
θ_x	mrad	0.16	0.04	73 %
θ_y	mrad	0.36	0.12	65 %
θ_s	mrad	0.56	0.22	60 %
Max load	kN	19.9	22.3	
Safety factor (static nominal loads)		15.5	12.5	
Heat flux @ 4.5 K	W	2.16	0.44	80 %
Compressor input power	kW	10.2	2.08	80 %

Both optimized solutions meet the stiffness requirements (Table 3.1). Solution 8S is generally more rigid, showing improvements of 20 %–73 % across most *DOF*s compared to 6S, with the exception of e_x, where it is 4 % less stiff. Structurally, both solutions are robust, with average safety factors of 15.5 for 6S and 12.5 for 8S. Additionally, the use of *CFRP* in the 8S design significantly reduces the heat load, requiring up to 80 % less power to extract heat at 4.5 K.

Table 4.6

List of fundamental parameters and their variation ranges considered as input parameters for the sensitivity analysis

Fundamental parameter	**6S**	**8S**	**value** (3σ)	
Equivalent diameter of a support	YES	YES	0.1	mm
Length of a support	YES	YES	0.1	mm
Elastic modulus of material	YES	YES	5	%
Position measurements uncertainty	YES	YES	0.15	mm
Sensibility of positioning system	YES	NO	0.05	mm
Pre-load	YES	YES	5	%

4.6.1. Sensitivity analysis

The sensitivity of the two support configurations to variations in input parameters has been analyzed. Some input parameters are fundamental, while others (e.g., support contraction) are derived from them. A list of the fundamental parameters and their variation ranges is provided in Table 4.6.

Random variations in these inputs can lead to:

- deformation of support elements;
- deformation of the vacuum vessel due to loads from the supports;
- deformation of the vacuum vessel caused by the pre-load system;
- displacements during the cool-down process;
- tolerance stack-up throughout the assembly chain, from the main structure to the cold mass.

Compared to the complete list in Table 4.1, the following effects are excluded from this analysis:

- backlash, which is assumed to be mitigated by the pneumatic pre-load system (Subsection 4.5.2);
- deformation of the main structure, as it does not influence the comparison between different cold mass supporting systems;
- deformation of the vacuum vessel due to differential pressure and self-weight, which are considered second-order effects.

Quantitative results of the sensitivity analysis of the 6S and 8S supporting systems in response to variations of input parameters (Table 4.6) are reported in Table 4.7 and Table 4.8. Overall the exactly constrained solution (6S) seems more sensitive to variations of input parameters. The axial internal actions on supports seem to be almost equally influenced, with 104 N of standard deviation (1σ) on average for the 6S supporting system and 90 N (1σ) for the 8S supporting system.

The impact of the design choices proposed in this Thesis on the beam transported through the gantry beam transfer line has been assessed in collaboration with experts from the Italian *CNAO* (national center of oncological hadron therapy). In addition to the deformations of the supports and cryostat computed using the developed *LPM*s, and the random errors estimated in the previously reported sensitivity analysis, the author also included the deformation of the main gantry structure. These results were used to optimize the positioning of the transfer line elements to enhance the effectiveness of beam corrections.

Table 4.7

Results of the sensitivity analysis for both the 6S and 8S supporting system. 1σ standard deviation of the internal axial action for each of the supports

	Rod1	Rod2	Rod3	Rod4	Rod5	Rod6	Rod7	Rod8	
Force Std. 1σ (6S)	97.08	89.55	120.85	134.62	93.55	90.60			N
Force Std. 1σ (8S)	86.64	86.96	87.16	86.83	93.90	93.57	93.71	94.10	N

Table 4.8

Results of the sensitivity analysis for both the 6S and 8S supporting system. 1σ standard deviation of the position and rotation of the cold mass

DOF	e_x	e_y	e_z		θ_x	θ_y	θ_z	
Pose Std. 1σ (6S)	0.28	0.06	0.13	mm	0.37	0.51	0.15	mrad
Pose Std. 1σ (8S)	0.02	0.02	0.02	mm	0.02	0.02	0.02	mrad

Performance metrics for the transfer line include the beam envelope radius at various gantry positions and the percentage of correction kicks exceeding the hardware limits of correctors currently used at *CNAO*. The full methodology is described in [69]. Beam envelope results are shown in Fig. 4.22 and Fig. 4.23, based on thousands of *MADX* simulations assuming the random error distributions described earlier. The maximum envelope, considering both the full data set (100th percentile) and the 95th percentile, indicates that solution 8S leads to a smaller envelope under the current sensitivity assumptions: 24.3 mm for 6S and 18.8 mm for 8S. Both stay within the beam envelope requirement of 26.7 mm, based on the good field region of the superconducting dipoles [70] (taken as 2/3 of the magnet bore radius).

The percentage of correction kicks exceeding current hardware capabilities reflects the likelihood of uncorrectable beam errors and potential beam losses. This percentage is 2.5 % for solution 6S and zero for solution 8S, indicating that solution 6S may result in beam losses without hardware upgrades or additional alignment measures, while solution 8S offers greater stability under current alignment assumptions.

4.6.2. Analysis of transportation and handling loads

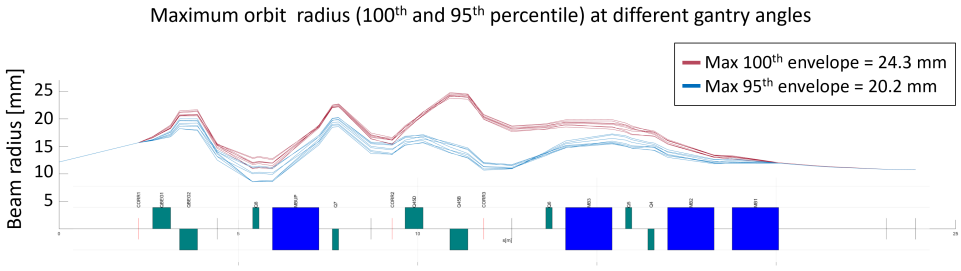

Fig. 4.22. Beam envelope in transfer line based on 6S supporting architecture. Results: courtesy of CNAO.

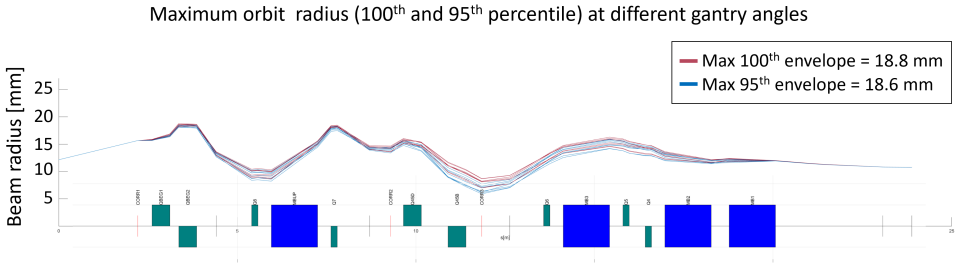

Fig. 4.23. Beam envelope in transfer line based on 8S supporting architecture. Results: courtesy of CNAO.

This section evaluates the performance of the 6S and 8S supporting systems under transportation and handling loads, where additional accelerations along x, y, and z may exceed those during nominal operation. The figure of merit is the minimum safety factor across all supports under various loading conditions. Transportation scenarios include road, rail, ship, and crane handling. Based on literature sources [71], [72], conservative acceleration values have been selected: 4.5 G (sideway), 5.6 G (longitudinal), and 9.5 G (vertical), each acting bidirectionally, defining six load cases listed in Table 4.9.

Table 4.9

Load cases considered for transportation and handling loads. G is the standard value for Earth gravity

Load cases	*LPM* dir.	Case 1	Case 2	Case 3	Case 4	Case 5	Case 6	
Sideway	x	4.5	0	0	−4.5	0	0	G
Longitudinal	y	0	5.6	0	0	−5.6	0	G
Vertical	z	−1	−1	8.5	−1	−1	−10.5	G

Results are shown in Fig. 4.24. Load case 6 is the most critical for both systems, yielding minimum safety factors of approximately 2.3 for 6S and 6.3 for 8S. The 8S solution thus offers a 2.7-times higher safety margin. Its high symmetry ensures uniform load distribution among supports, and the use of *CFRP* provides superior mechanical strength compared to titanium. Both systems are deemed safe for transport, as lower safety factors are acceptable without high-cycle fatigue. Nevertheless, 6S could benefit from a temporary auxiliary support system during transport, a common practice in cryostat logistics.

4.6.3. Analysis of natural frequencies of the systems

The natural frequencies of the 6S and 8S solutions were compared for the first dipole of the gantry beam line using *FEA*. The simulation workflow involves a steady-state thermal analysis to obtain the temperature distribution, followed by a static structural analysis to determine the stress state after cool-down, which is then used in a modal analysis to compute natural frequencies and participation factors γ_i (in *ANSYS* notation). The ratio of the dipole mass to the total mass (or inertia, for rotations) is used to ensure all major modes of the cold mass are captured in the comparison.

Solution 8S generally exhibits higher natural frequencies, though the difference is not substantial. It also displays a more decoupled dynamic behavior: modes 1–5 represent rigid-body motion of the dipole, as their $M_{eff,i}/M_{TOT}$ values exceed the dipole-to-total

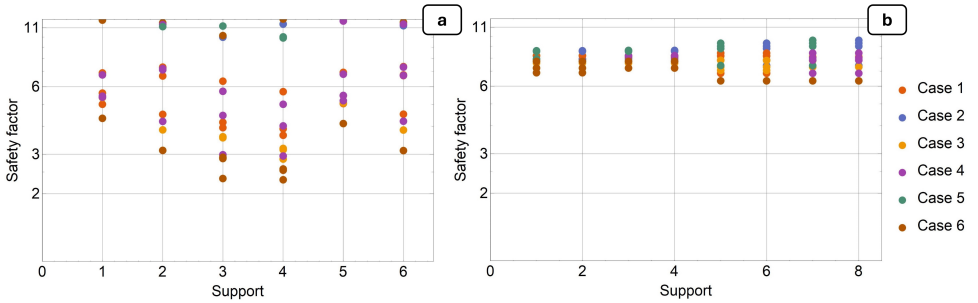

Fig. 4.24. Results of the safety factor for each rod in supporting system 6S (**a**) and 8S (**b**) for the different transportation and handling load cases.

mass ratio, with no significant coupling in other *DOF*s. These preliminary results suggest both solutions have comparable dynamic characteristics, though further optimization may be necessary to eliminate low-frequency modes before testing and prototyping.

4.6.4. Comparative analysis conclusions

The optimized 6S and 8S supporting systems have been compared in terms of accuracy under load during gantry rotation, heat-flux through supports, sensitivity to input variations, transportation and handling performance, and natural frequencies. With the exception of natural frequencies, which are comparable between the two, solution 8S outperforms 6S overall.

Thanks to the adoption of *CFRP* in 8S, the conductive heat-flux at 4.7 K is significantly reduced from 2.16 W (6S) to 0.44 W (8S), leading to a decrease in required cooling power from 10.2 kW to 2.08 kW. In terms of accuracy, 8S shows improved performance with error reductions between 20 % and 73 % due to lower elastic deformation during rotation.

A sensitivity analysis was performed to evaluate how uncertainties in input parameters (e.g., material properties and assembly tolerances) affect system performance. Standard deviations in all six *DOF*s were used as the metric, showing that solution 8S is about ten times less sensitive than 6S. This improved robustness stems from the smaller cool-down displacements in 8S, which limit the propagation of room-temperature uncertainties.

Solution 6S, however, has the advantage of potential automation: its exactly constrained architecture enables automated positioning of the warm prismatic joints, already feasible in the current design. Through active control, this could compensate for elastic deformations in both the cryostat and the gantry structure, reducing sensitivity to uncertainties and allowing relaxed rigidity requirements, thus enabling significant weight savings in the gantry.

Under transportation and handling loads, solution 8S also performs better. Thanks to its symmetry, the supports are more uniformly loaded, yielding a higher safety margin. For extreme load cases (accelerations of 5.6 G longitudinal, 4.5 G sideway, and 10.5 G vertical), the minimum safety factor is 2.3 for 6S and 6.3 for 8S.

In conclusion, for the rotating gantry application in medical treatments, solution 8S is deemed superior if automation is excluded. However, if active positioning is implemented, solution 6S can become highly advantageous, enabling not only recovery of cryostat deformations but also compensation of gantry deflections, opening the door to lighter and more efficient machine designs.

Conclusions

This Thesis contributes to the mechanical engineering field by proposing a novel model that can be used to design and optimize the rod supporting system of cryogenic devices under a generic variable load. Through a comprehensive literature review and original structured mathematical modeling, it identifies and addresses a key gap in the design of support systems under general variable load conditions. Two alternative support architectures– one statically determinate (6S), the other over-constrained (8S)– are proposed, mathematically modeled, validated and optimized. The resulting insights not only advance the state of the art in support system design but also provide tools that can be generalized to a range of cryogenic applications such as: accelerator cryogenic components that can be developed in the future, superconducting radio frequency cavities, optical alignment systems for cryogenic devices in high-energy physics experiments, superconducting generators for wind turbines, and supporting systems in the space industry.

Key findings in this Thesis include:

1. The novel mathematical lumped parameter models (*LPM*s) are adaptable to a wide range of rod support configurations (six or more rods) and enable rapid evaluation of system performance, such as position of the cryogenic device and load distributions in supports.
2. The *LPM*s describe supporting systems that are arranged in configurations not necessarily symmetric, and can model a system where supports have their own dimensions and material, which may differ from one another.
3. The *LPM*s show strong agreement with *FEA* results, achieving accuracies of 98.6 % and 99.4 % for the general 8 and 11-support models. Accuracies of 97–98.5 % have been achieved for solution 6S and 8S designed for the gantry study case.
4. The proposed *LPM*s outperform *FEA* in terms of calculation speed by 20 times, measurement achieved running the *LPM* and *FEA* on the same hardware.
5. Optimization using a parallel genetic algorithm resulted in notable performance gains over manually optimized designs in the specific case of the gantry application, particularly in position accuracy robustness and thermal efficiency. The computer aided optimized solution has been proven to be by average 16 % and up to 83 % better in terms of accuracy during the rotation of the gantry. The computer aided optimized solution has been proven to require half of the pre-load needed by the initial designed supporting system to eliminate backlash. This translates into a reduction of about 44 % of the internal actions in the supports and, consequently, of the heat-flux for the optimized 6S configuration. The heat-flux reduction allows a reduction from 19.2 kW to 10.4 kW of the power needed by compressors in the cooling system of the machine.

This study contributes to the cryogenic device engineering field by providing a validated, wide modeling framework; qualitative advantages with respect to classical *FEA* analysis include:

1. Simplicity of the model. Thanks to the limited set of essential parameters in the *LPM*, the model can be used by a wider community of designers and engineers, allowing to achieve accurate results almost independently from the level of expertise that is instead highly required to run accurate *FEA* analysis.

2. Insightfulness of the model. Thanks to its simplicity, the developed *LPM* offers clear direct insights into the fundamental relationships that govern the system. Designers and engineers can have a faster and clearer grasp on the influence of relevant parameters on crucial output quantities, boosting the capability to choose optimal configurations of supports before running computationally expensive *FEA*.

The developed model can be used for fast, flexible evaluation of symmetric and non-symmetric rod supporting structures in cryogenic environments subject to non-variable and variable loads. **Possible evaluations** include:

1. Large-scale sensitivity studies, by varying the most relevant driving parameters of the design and addressing the impact of their variations to the mechanical system performances and, in case of accelerator technologies, the crucial impact of such variations on accelerator beam parameters.
2. Material and geometric optimization strategies that balance structural performance with thermal load constraints and can be easily tuned to optimize other target quantities by introducing new objective functions in the proposed optimization algorithm.
3. Support arrangement optimization that includes realistic boundaries given by mechanical system integration.

The modeling, optimization, and comparison strategies developed in this Thesis extend beyond the specific case of superconducting magnets for hadron therapy. They reflect a more general design philosophy centered on computationally efficient modeling tools that enable deep exploration of complex, highly constrained engineering problems.

The proposed and validated LPM framework supports a shift away from common approaches based just on experience and trial-and-error approaches based on finite element methods toward more digitally assisted designs. In particular, the ability to evaluate thousands of configurations in a fraction of the time required by traditional FEA enables early-stage exploration of design spaces that were previously impractical to be fully assessed. This capability is especially relevant in fields where mechanical performance must be balanced with thermal, vibrational, and integration constraints, such as in accelerator technologies, space systems, superconducting generators or motors, and high-energy physics experiments.

Finally, the Thesis demonstrates the value of tightly coupling the model, optimization, and validation, which is a workflow that aligns with current trends in digital twin development. By implementing performance evaluation and sensitivity analysis directly into the design loop, the methods developed here offer a foundation for more agile, iterative designs.

Results of this Thesis has contributed considerably to one of the milestones (M7.2) of the Horizon2020 European project heavy ion therapy research integration plus (HITRI*plus*), by proposing the supporting system designed and reported in this Thesis as baseline for the carbon-ion gantry mechanical design and integration. This Thesis has been used to analyzed the impact of the mechanical solutions proposed on the optimization of the beam optics layout aiming at correcting the random errors calculated in the sensitivity studies presented in the Thesis. **Notable results for the gantry** study case are:

1. Solution 8S for the applicative case of the rotating gantry, incorporating CFRP supports, outperforms Ti6Al4V solution 6S in metrics, such as accuracy performances under load during the rotation of the machine, heat-flux through supports,

sensitivity to variations of input parameters, and performance during transportation/handling phases, in case automation is not considered, while 6S retains potential advantages in automated systems due to its simpler architecture, tunability and reduced stress state induced in the cryogenic device.
2. Solutions 6S and 8S have been proven compliant to beam requirements by beam tracking ensuring the efficacy of correcting errors related to deformations and manufacturing tolerances without major beam losses.

While this Thesis presents a validated modeling, some **limitations** must be acknowledged:

1. The developed LPMs are applicable to a specific class of supporting architectures that employ only rods connected through spherical or universal joints. Nonetheless, this architectural class is among the most commonly adopted, as highlighted in the literature review. This limits the applicability of the models in configurations where the supports are connected through joint types that introduce significant rotational constraints.
2. The modeling approach assumes the absence of friction. However, this can be solved already by introducing a more complete model.
3. The validation of the models has been conducted primarily through numerical comparison with FEA. While the agreement is strong, experimental validation through physical prototyping and testing must be foreseen. Real-world boundary conditions, assembly tolerances, and material imperfections may affect the performance in ways that may differ from the current hypothesis.

These limitations define the current boundaries of the proposed methodology and provide motivation for **future developments** which may include:

1. The extension of the proposed *LPM*s to supporting systems that utilize supports other than linking rods (joined solely by universal and spherical joints) by including the contribution of bending and torsion in the response of the system. This extension can be used to simulate the impact of friction, modeling it as additional torsional or bending stiffness.
2. The integration of the calculation of the natural frequencies of the system enabling the introduction of fitness functions to fine-tune the system's frequency response during optimization with the genetic algorithm.
3. The study of the stress-state on the cryogenic device generated by the over-constrained system.
4. The completion of the validation process, although the *LPM*s have already been deemed as reliable as *FEA*s, through a prototyping and testing campaign.

The most relevant outcome of this Thesis is, therefore, the novel mathematical model developed for rod supporting systems applied to cryogenic devices. It combines simplicity in terms of the number of relevant parameters with low computational cost and high accuracy compared to standard *FEA*s. These advantages make it accessible to a wider community than just experienced finite element analysts, providing useful insights into possible ways of optimizing the supporting system.

Acronyms

ATLAS	a toroidal *LHC* apparatus (*LHC* collaboration)
BT	barrel toroid
CAS	Chinese Academy of Sciences
CFRP	carbon fibre reinforced polymer
CMS	compact muon solenoid (*LHC* experiment)
CNAO	national center of oncological hadron therapy
CS	central solenoid
DEMO	demonstration power plant
DOF	degrees of freedom
DPK	direct position kinematics
ECT	end cap toroid
ELI	extra low interstitial
ESS	European Spallation Source
FAIR	Facility for Antiproton and Ion Research
FEA	finite element analysis
FPC	fundamental power coupler
GA	genetic algorithm
GFRE	glass fibre reinforced epoxy
HIE-ISOLDE	high intensity and energy *ISOLDE*
HITRIplus	heavy ion therapy research integration plus
HL-LHC	high luminosity *LHC*
ICS	inter-cavity support
IHEP	Institute of High Energy Physics of *CAS*
IPK	inverse position kinematics
ISOLDE	isotope separator on line device
ITER	International Thermonuclear Experimental Reactor
LCLS-II	Linac Coherent Light Source II
LHC	Large Hadron Collider
LPM	lumped parameter model
MDS	magnetic density separator
MICE	Muon Ionization Cooling Experiment
MRI	magnetic resonance imaging
Mu2e	muon-to-electron conversion
RHIC	Relativistic Heavy Ion Collider
SPL	superconducting proton linac
SSC	Superconducting Super Collider
SSRF	Shanghai Synchrotron Radiation Facility

SSS	short straight section
TLS	Taiwan Light Source
UFGE	unidirectional fibreglass epoxy
UT	University of Twente
VECC	Variable Energy Cyclotron Centre

Bibliography

[1] Alberto Martín-Martín et al. “Google Scholar, Web of Science, and Scopus: A systematic comparison of citations in 252 subject categories”. In: *Journal of informetrics* 12.4 (2018), pp. 1160–1177.

[2] Yiyong Liu et al. “Design of cold mass supports for a superconducting undulator prototype at SINAP”. In: *IEEE Transactions on Applied Superconductivity* 25.3 (2014), pp. 1–4.

[3] Li Wang et al. “Development of a Test Cryostat for a Superconducting Undulator Prototype at the SSRF”. In: *IEEE Transactions on Applied Superconductivity* 31.5 (2021), pp. 1–5.

[4] G. Olivier et al. “Ess cryomodules for elliptical cavities”. In: *Proceedings of the 16th International Conference on RF Superconductivity*. 2013.

[5] Christine Darve et al. “The ESS elliptical cavity cryomodules”. In: *AIP Conference Proceedings*. Vol. 1573. 1. American Institute of Physics. 2014, pp. 639–646.

[6] *European Spallation Source*. European Spallation Source. URL: https://europeanspallationsource.se/article/2023/03/15/ess-installs-first-two-cryomodules-linac (visited on 04/19/2023).

[7] Laura Monaco et al. “Fabrication and treatment of the ESS medium beta prototype cavities”. In: *Proc. IPAC’17* (2017).

[8] Federico Carra et al. “Assessment of thermal loads in the CERN SPS crab cavities cryomodule1”. In: *Journal of Physics: Conference Series*. Vol. 874. 1. IOP Publishing. 2017, p. 012005.

[9] Thomas Jones et al. “Development of a Novel Supporting System for High Luminosity LHC SRF Crab Cavities”. In: *18th Int. Conf. on RF Superconductivity (SRF’17), Lanzhou, China, July 17–21, 2017*. JACOW, Geneva, Switzerland. 2018, pp. 304–308.

[10] Shrikant Pattalwar et al. “Key Design Features of Crab-Cavity Cryomodule for HiLumi LHC”. In: (2014).

[11] P. Azevedo. *SPL Short Cryomodule Design*. URL: https://indico.cern.ch/event/216370/contributions/441396/attachments/345704/482100/SPL_SC_Design_PAzevedo_SPLmeeting_7_12_2012.pdf (visited on 04/19/2023).

[12] V. Parma et al. *Status of the Superconducting Proton Linac (SPL) cryo-module*. Tech. rep. 2014.

[13] S. Atieh et al. *Mechanical design and fabrication studies for SPL superconducting RF cavities*. Tech. rep. 2011.

[14] Sebastien Bousson et al. “The ESS spoke cavity cryomodules”. In: *AIP Conference Proceedings*. Vol. 1573. 1. American Institute of Physics. 2014, pp. 665–672.

[15] P. Duthil et al. “Design and Prototyping of the Spoke Cyromodule for ESS”. In: *HB2016, WEAM4Y01* (2016).

[16] Denis Reynet et al. “Design of the ESS Spoke cryomodule”. In: *MOP089, SRF* (2013).

[17] U. Bhunia et al. “Development and performance evaluation of a conduction-cooled warm bore HTS steering magnet”. In: *Physica C: Superconductivity and its Applications* 604 (2023), p. 1354191.

[18] Jun-Sheng Zhang et al. “Magnetic and thermal design of HTS quadrupole magnet for newly developed superconducting proton cyclotron beam line”. In: *Journal of Superconductivity and Novel Magnetism* 32 (2019), pp. 529–538.

[19] J. J. Kosse et al. “Mechanical design of a superconducting demonstrator for magnetic density separation”. In: *Superconductor science and technology* 34.11 (2021), p. 115019.

[20] N. Delruelle et al. “The high Beta cryo-modules and the associated cryogenic system for the HIE-ISOLDE upgrade at CERN”. In: *AIP Conference Proceedings*. Vol. 1573. 1. American Institute of Physics. 2014, pp. 811–818.

[21] Y. Kadi, M. A. Fraser, and A. Papageorgiou-Koufidou. *HIE-ISOLDE: technical design report for the energy upgrade*. Ed. by Y. Kadi. CERN Yellow Reports: Monographs. Geneva: CERN, 2018. DOI: 10.23731/CYRM-2018-001. URL: http://cds.cern.ch/record/2635892.

[22] Miao-Fu Xu et al. “Design, assembly, and pre-commissioning of cryostat for 3W1 superconducting wiggler magnet”. In: *Nuclear Science and Techniques* 31 (2020), pp. 1–15.

[23] H. H. Chen et al. “Design of mechanical structure and cryostat for IASW superconducting wiggler at NSRRC”. In: *2007 IEEE Particle Accelerator Conference (PAC)*. IEEE. 2007, pp. 374–376.

[24] C-S. Hwang et al. “Superconducting wiggler with semi-cold beam duct at Taiwan light source”. In: *Nuclear Instruments and Methods in Physics Research Section A: Accelerators, Spectrometers, Detectors and Associated Equipment* 556.2 (2006), pp. 607–615.

[25] Li Wang et al. “Design and analysis of a self-centered cold mass support for the MICE coupling magnet”. In: *IEEE transactions on applied superconductivity* 21.3 (2011), pp. 2259–2262.

[26] Egbert Fischer et al. “Superconducting quadrupole module system for the sis100 synchrotron”. In: *Proc. RUPAC*. 2012, pp. 143–145.

[27] J. P. Meier et al. “Cryo-technical design aspects of the superconducting SIS100 quadrupole doublet modules”. In: *AIP Conference Proceedings*. Vol. 1573. 1. American Institute of Physics. 2014, pp. 1519–1526.

[28] G. Ambrosio et al. “Challenges and design of the transport solenoid for the Mu2e experiment at Fermilab”. In: *IEEE transactions on applied superconductivity* 24.3 (2013), pp. 1–5.

[29] Mauricio Lopes et al. “Mu2e transport solenoid cold-mass alignment issues”. In: *IEEE Transactions on Applied Superconductivity* 27.4 (2017), pp. 1–5.

[30] J. H. Sondericker and L. J. Wolf. “Alternative concepts for structurally supporting the cold mass of a superconducting accelerator magnet”. In: *Supercollider 3*. Springer, 1991, pp. 175–189.

[31] P. Wanderer et al. “Construction and testing of arc dipoles and quadrupoles for the Relativistic Heavy Ion Collider (RHIC) at BNL”. In: *Proceedings Particle Accelerator Conference*. Vol. 2. IEEE. 1995, pp. 1293–1297.

[32] Lankai Li et al. “Theoretical model of a cold mass strap suspension system for superconducting magnets”. In: *IEEE transactions on applied superconductivity* 21.6 (2011), pp. 3640–3645.

[33] Akira Yamamoto et al. “The ATLAS central solenoid”. In: *Nuclear Instruments and Methods in Physics Research Section A: Accelerators, Spectrometers, Detectors and Associated Equipment* 584.1 (2008), pp. 53–74.

[34] T. H. Nicol, R. C. Niemann, and J. D. Gonczy. “SSC magnet cryostat suspension system design”. In: *Advances in Cryogenic Engineering*. Springer, 1988, pp. 227–234.

[35] Arnaud Devred et al. *Quench characteristics of full-length SSC R&D dipole magnets*. Springer, 1990.

[36] Thomas Peterson et al. “LCLS-II 1.3 GHz cryomodule design-modified tesla-style cryomodule for CW operation”. In: *Proc. 17th Int. Conf. RF Superconductivity (SRF’15)*. 2015, pp. 1417–1421.

[37] John N. Galayda et al. “The LCLS-II: A high power upgrade to the LCLS”. In: *9th IPAC* (2018), p. 18.

[38] Kun Lu et al. “Evolution of the design of cold mass support for the ITER magnet feeder system”. In: *Plasma Science and Technology* 15.2 (2013), p. 196.

[39] Yinfeng Zhu et al. “Conceptual design and analysis of cold mass support of the CS3U feeder for the ITER”. In: *Plasma Science and Technology* 15.6 (2013), p. 599.

[40] Fabien Seyvet et al. “Improvement of the geometrical stability of the LHC cryo-dipoles when blocking the central support post”. In: *Proceedings of the 2005 Particle Accelerator Conference*. IEEE. 2005, pp. 2675–2677.

[41] M. Mathieu et al. “Supporting systems from 293 K to 1.9 K for the Large Hadron Collider (LHC) cryo-magnets”. In: *Advances in cryogenic engineering* (1998), pp. 427–434.

[42] Jishnu Dwivedi et al. *The alignment jacks of the LHC cryomagnets*. Tech. rep. 2004.

[43] M. Castoldi et al. *Thermal performance of the supporting system for the Large Hadron Collider (LHC) superconducting magnets*. Tech. rep. 1999.

[44] A. Dudarev et al. “First full-size ATLAS barrel toroid coil successfully tested up to 22 kA at 4 T”. In: *IEEE transactions on applied superconductivity* 15.2 (2005), pp. 1271–1274.

[45] C. Mayri et al. “Suspension system of the barrel toroid cold mass”. In: *IEEE transactions on applied superconductivity* 16.2 (2006), pp. 525–528.

[46] J. P. Badiou et al. *ATLAS barrel toroid: Technical Design Report*. Technical design report. ATLAS. Electronic version not available. Geneva: CERN, 1997. DOI: 10.17181/CERN.RF2A.CP5T. URL: http://cds.cern.ch/record/331065.

[47] F. Nunio et al. “Mechanical design of the Iseult 11.7 T whole body MRI magnet”. In: *IEEE Transactions on Applied Superconductivity* 20.3 (2010), pp. 760–763.

[48] P. Vedrine et al. “Latest progress on the Iseult/INUMAC whole body 11.7 T MRI magnet”. In: *IEEE transactions on applied superconductivity* 22.3 (2011), pp. 4400804–4400804.

[49] Nicolas Boulant and Lionel Quettier. “Commissioning of the Iseult CEA 11.7 T whole-body MRI: current status, gradient–magnet interaction tests and first imaging experience”. In: *Magnetic Resonance Materials in Physics, Biology and Medicine* (2023), pp. 1–15.

[50] D. Elwyn Baynham et al. “Engineering design optimisation of the superconducting end cap toroid magnets for the ATLAS experiment at LHC”. In: *IEEE transactions on applied superconductivity* 9.2 (1999), pp. 856–859.

[51] D. E. Baynham et al. “ATLAS end cap toroid final integration, test and installation”. In: *IEEE transactions on applied superconductivity* 18.2 (2008), pp. 391–394.

[52] *ATLAS end-cap toroids: Technical Design Report*. Technical design report. ATLAS. Electronic version not available. Geneva: CERN, 1997. DOI: 10.17181/CERN.P03D.WQLV. URL: http://cds.cern.ch/record/331066.

[53] B. Levesy et al. “Design and test of the titanium alloy tie rods for the CMS coil suspension system”. In: *IEEE transactions on applied superconductivity* 12.1 (2002), pp. 403–406.

[54] N. Mitchell et al. “The ITER magnets: Design and construction status”. In: *IEEE transactions on applied superconductivity* 22.3 (2011), pp. 4200809–4200809.

[55] Min Liao et al. “Prototype engineering test platform of ITER magnet gravity support”. In: *Plasma Science and Technology* 15.2 (2013), p. 192.

[56] V. Corato et al. “The DEMO magnet system–Status and future challenges”. In: *Fusion engineering and design* 174 (2022), p. 112971.

[57] Luca Piacentini et al. “Literature Review of Suspension Systems for Superconducting Elements”. In: *Machines* 11.10 (2023). ISSN: 2075-1702. DOI: 10.3390/machines11100929. URL: https://www.mdpi.com/2075-1702/11/10/929.

[58] Xin-Jun Liu and Jinsong Wang. “Parallel kinematics”. In: *Springer Tracts in Mechanical Engineering* (2014).

[59] Matteo-Claudio Palpacelli et al. “Functional Design of a 6-DOF Platform for Micro-Positioning”. In: *Robotics* 9.4 (2020), p. 99.

[60] Giovanni Legnani et al. “A new isotropic and decoupled 6-DoF parallel manipulator”. In: *Mechanism and Machine Theory* 58 (2012), pp. 64–81.

[61] Luca Piacentini et al. “Design of a 6-supports exactly constrained supporting system for superconducting magnets and its application to rotating gantries for cancer therapy”. In: *Meccanica* (2024), pp. 1–24.

[62] Colin Caprani. *Virtual Work 3rd Year Structural Engineering*. 2010. URL: https://www.colincaprani.com/files/notes/SAIII/Virtual%20Work%201011.pdf (visited on 10/23/2024).

[63] Sanjay Govindjee. *Engineering mechanics of deformable solids: a presentation with exercises*. Oxford University Press, USA, 2012.

[64] Luca Piacentini et al. “Lumped Parameter Model for Structural Analysis of Over-Constrained Multi-Legged Parallel Mechanism Supporting System Applied to Cryogenic Devices.” In: *Machines* 13.2 (2025).

[65] National Institute of Standards and Technologies. *Properties of solid materials from cryogenic to room-temperatures*. URL: https://trc.nist.gov/cryogenics/materials/materialproperties.htm (visited on 04/19/2023).

[66] Stephanie Forrest. “Genetic algorithms”. In: *ACM computing surveys (CSUR)* 28.1 (1996), pp. 77–80.

[67] Darrell Whitley, Soraya Rana, and Robert B Heckendorn. “The island model genetic algorithm: On separability, population size and convergence”. In: *Journal of computing and information technology* 7.1 (1999), pp. 33–47.

[68] Patxi Duthil. “Material properties at low temperature”. In: *arXiv preprint arXiv:1501.07100* (2015).

[69] Simone Savazzi et al. “Optimization of a carbon-ion gantry layout based on simulated mechanical errors”. Under submission.

[70] M. G. Pullia et al. “Gantries for carbon ions”. In: *Health and Technology* (2024), pp. 1–11.

[71] *Transport Information Service*. German Insurance Association. URL: https://www.tis-gdv.de/tis_e/verpack/verpackungshandbuch/03verpackungshandbuch_0131-htm/ (visited on 01/10/2025).

[72] Péter Böröcz. “Vibration and acceleration levels of multimodal container shipping physical environment”. In: *Packaging Technology and Science* 32.6 (2019), pp. 269–277.

Luca Piacentini was born in 1996 in Brescia, Italy. He obtained his Bachelor's degree in Mechanical and Industrial Engineering and a Master's degree in Mechanical Engineering (2021) from the University of Brescia. Since 2021, he has been a research assistant at Riga Technical University and carried out his research mainly abroad, at CERN. He is currently a Project Engineer at T.I.S. Service S.p.A. His research interests include mechanical design and system optimisation in social applications.